博士論文

走査プローブ顕微鏡による DNA の高分解能観察

前田　泰

大阪大学大学院

理学研究科

High resolution Imaging of DNA using scanning probe microscopy

The Institute of Scientific and Industrial Research
Osaka University

Yasushi Maeda

Contents

Chapter 1

General Introduction

Chapter 1

General Introduction

1.1 Background of this study

Five years after the invention of the scanning tunneling microscopy (STM) [1], the atomic force microscopy (AFM) was invented [2] as a new technique of the scanning probe microscopy (SPM). The AFM made it possible to observe the surface of insulators with nano-scale, which was not possible with the STM. The AFM has thus achieved a rapid development as a technique of observation and evaluation for organic materials including bio-materials.

DNA is one of the most interesting and important molecules for humankind because it carries genetic information. Since the first successful imaging of DNA molecules with AFM in 1989 [3], many research groups have performed AFM observation of DNA [4-7]. However, any study has not achieved the high resolution imaging of the periodic microstructure of the double helix because of the limitation of the resolution of the AFM, i.e. ten nanometers. This structure has been successfully observed only by using the hydration scanning tunneling microscopy [8] and the low-temperature STM using pulse injection method under UHV conditions [9,10]. Despite such achievements, AFM imaging of DNA remains a highly desirable goal in the field of SPM since AFM can offer strong advantage for imaging of insulative and bulky macromolecules.

True atomic resolution was achieved by noncontact atomic force microscopy (NC-AFM) in 1995 [11]. Several groups have succeeded in obtaining atomically resolved images of well-defined clean surfaces [12, 13].

Recently, this technique has been applied to various surfaces including oxides [14] and organic layers [15]. In such case, the interaction between tip and sample is considered to arise from van der Waals force, electrostatic force and covalent bonding interaction [16]. However, the imaging mechanism of NC-AFM is still unclear even in the case of well-defined surfaces.

1.2 Purpose of the present study

Obtaining high resolution images of DNA is much more difficult than that of well-defined surfaces mainly because of following reasons: Adhesion forces, which originate from a water and/or organic contamination layer caused by wet processes used for preparation of DNA samples, are present even under ultrahigh vacuum conditions [17]. This force seriously affects the NC-AFM observation. Additionally, because of the large protrusion of DNA, AFM tips must be extremely sharp for obtaining high resolution images.

The purpose of the present study is the observation of double helix structure of DNA using NC-AFM. As described in chapter 3, single- and double-stranded DNA on mica surface were successfully observed by NC-AFM in spite of the presence of the strong adhesion force on the surface. The detailed structures of the DNA molecules were observed indicating higher resolution of NC-AFM than that of other AFM modes. Furthermore, it was found that contrast artifacts give various detailed structures.

In chapter 4, high resolution imaging is described that was performed on Cu(111) surface with shape-controlled tip using NC-AFM. In this system, imaging of the double helix structure has been achieved. The most

frequently observed values of the pitch lengths (3-4 nm) are consistent with that of the Watson-Crick model (3.4 nm). However, the observed pitch lengths are widely distributed in the range of 2-7 nm and the observed height of 1 nm is half of the height in Watson-Crick model (2nm), suggesting deformation of DNA on the surface.

In chapter 5, the multi-mode SPM observation is described that is carried out on Cu(111) surfaces using a conductive cantilever. In this mode, the STM and the NC-AFM images can be obtained simultaneously. The multi-mode SPM observation has revealed the relationship between the STM image and the topography of DNA molecules, suggesting that the density of states of DNA is two order smaller than that of Cu(111) surface. This result indicates the potential of the multi-mode SPM to make clear the electronic properties of DNA molecules.

1.3 References

[1] G. Binning, H. Rohrer, C. Gerber, E. Weibel: Phys. Rev. Lett. **49** (1982) 57 and Appl. Phys. Lett. **40** (1982) 178.

[2] G. Binning, C.F. Quate, C. Gerber: Phys. Rev. Lett. **56** (1986) 930.

[3] S.M. Lidsay, L.A. Nagahara, T. Thundat, U. Knipping, R.L. Rill, B. Dark, C.B. Prater, A.L. Weisenhorn, S.A.C. Gould, P.K. Hansma: J. Biomol. Struc. Dynami. **7** (1989) 279.

[4] H.G. Hansma, I. Revenko, K. Kim, D.E. Laney: Nucleic Acids Res. **24** (1996) 713.

[5] H.G. Hansma, D.E. Laney, M. Bezanilla, R.L. Sinsheimer: Biophys. J. **68** (1995) 1672.

[6] H.G. Hansma, R.L. Sinsheimer, J. Groppe, T.C. Bruice, V. Elings, G. Gurley, M. Benzanilla, I.A. Mastrangelo, P.V.C. Hough, P.K. Hansma: Scanning **15** (1993) 296

[7] T. Thundat, D.P. Allison, R.J. Warmack: J. Vac. Sci. Technol. **A11** (1993) 824.

[8] M. Heim, R. Steigerwald, R. Guckenberger: J. Struc. Biol. **119** (1997) 212.

[9] T.Kanno, H. Tanaka, T. Nakamura, H. Tabata, T. Kawai: Jpn. J. Appl. Phys. **38** (1999) L606.

[10] H. Tanaka, C. Hamai, T. Kanno, T. Kawai: Surf. Sci. **432** (1999) L611.

[11] F. J. Giessibl: Science **267** (1995) 68.

[12] Y. Sugawara, M. Ohta, H. Ueyama, S. Morita: Science **270** (1995) 1646.

[13] S. Kitamura, M. Iwatsuki: Jpn. J. Appl. Phys. **35** (1996) L668.

[14] K. Fukui, H. Onishi, Y. Iwasawa: Phys. Rev. Lett. **79** (1997) 4202.

[15] K. Fukui, H. Onishi, Y. Iwasawa: Chem. Phys. Lett. **280** (1997) 296

[16] T. Uchihashi, Y. Sugawara, T. Tsukamoto, M. Ohta, S. Morita, M. Suzuki: Phys Rev. **B56** (1997) 9834.

[17] Y. Sugawara, M. Ohta, T. Konishi, S. Morita, M. Suzuki, Y. Enomoto: Wear **168** (1993) 13.

Chapter 2

Noncontact atomic force microscopy

Chapter 2

Noncontact atomic force microscopy

2.1 Overview

Atomic force microscopy (AFM) provides three-dimensional real space images of surfaces [1-3]. AFM images are obtained by scanning a tip over a surface with constant tip-sample interaction as shown in Fig. 2-1(a). The tip-sample interaction is related to deflection of a small lever (cantilever) which have a 100-200 μm length as illustrated in Fig. 2-1(b).

There are three modes in AFM operation, i.e. contact, tapping and noncontact mode. The detection methods of tip-sample interactions in these modes are different from each other. In contact-mode AFM, a tip contacts with surface statically as shown in Fig. 2-2(a). Tip-sample interaction (F) is related to the cantilever's deflection (Δz):

$$F=-k\Delta z$$

where k is cantilever's spring constant. An absolute value of F can be measured only in this mode.

In tapping mode AFM (TM-AFM), a cantilever is driven at fixed frequency, and tip-sample interaction is detected as variations in the amplitude (Fig. 2-2(b)). In this mode, the tip taps a surface periodically. This prevents moving a sample by scanning the tip.

In noncontact AFM (NC-AFM), a cantilever is driven at its resonance frequency by applying positive feedback. The tip-sample interaction is detected as shift of the cantilever's resonance frequency by frequency modulation (FM) technique [4]. This mode is the most sensitive in AFM for

detecting the tip-sample interaction. This allows us to keep tip-sample distance constant in attractive force (noncontact) region (Fig. 2-2(c)).

2.2 Theory of NC-AFM

The cantilever's oscillation in NC-AFM is described by the equation of motion:

$$m\ddot{z} + \alpha\dot{z} + kz + F(z) = F_0 \cos ft \qquad (1)$$

where α is a damping constant; F_0 and f are the amplitude and the frequency of driving force, respectively. F(z) is the force acting between tip and surface at the relative distance z. k and m are the spring constant and the effective mass of the cantilever, respectively.

Assuming small oscillation amplitude, the frequency shift (Δf), which is induced by the tip-sample interaction, is described as follows:

$$\Delta f = -\frac{f_0}{2k}\frac{dF}{dz} \qquad (2)$$

where $f_0=(k/m)^{1/2}$ is the resonance frequency of the free cantilever. In this case, frequency shift is proportional to the "force gradient". Actually, the small oscillation amplitude can not be assumed because typical oscillation amplitude is more than 10 nm. However, equation (2) is useful to understand the distance dependence of the frequency shift [5-8].

Assuming small interaction (F(z)), the frequency shift can be described using a perturbation theory [9]:

$$\Delta f \cong \frac{f_0}{2\pi kA}\int_0^{2\pi} F(z)\cos\theta\, d\theta \qquad (3)$$

where A is the oscillation amplitude. This equation indicate that the frequency shift is related to not only force acting F(z) and also the

oscillation amplitude A. This is more realistic than equation (2). The calculated frequency shift using equation (3) is in good agreement with that measured by NC-AFM [9-11].

2.3 Instrumentation of NC-AFM

In this study, NC-AFM was performed using UHV system as shown in Fig. 2-3. This system is composed of three chambers: (1) the growth chamber in which deposition of metal thin film and pulse injection of DNA are performed; (2) the preparation chamber for Ar ion sputtering; (3) the main and the SPM chamber in which the samples are stored and SPM observation is performed. The base pressures of the growth, preparation and SPM chamber are 10^{-8}, 10^{-8} and 10^{-9} Torr, respectively.

Fig. 2-4 is the block diagram of AFM/STM system. Using this system, we can perform NC-ATM (Chapter 3, 4) and multi-mode SPM (Chapter 5) observation. In NC-AFM, the cantilever is oscillated at its resonance frequency by applying positive feedback. The signal of cantilever's oscillation, detected by an optical reflection method, is put into the phase locked loop (PLL) circuit to detect the resonance frequency and the two-phase lock-in amplifier to detect the oscillation amplitude. Both of these signals can be used as a feedback signal. Feedback is applied to the Z piezo to maintain the frequency shift or oscillation amplitude constant.

In multi-mode SPM, tip-sample distance is controlled by the tunneling current using a conductive cantilever which is driven at its resonance frequency (~300 kHz). The tunneling current is averaged through STM pre-amplifier whose time constant is ~1 ms. The frequency shift is detected by the optical detection technique as mentioned above. The STM image and the

frequency shift image are simultaneously obtained in a scan using this operation mode [12].

2.4 References

[1] R. Wisendanger, H.-J. Guntherrodt: "*Scanning Tunneling Microscopy II*" Springer-Verlag

[2] R. Wisendanger, H.-J. Guntherrodt: "*Scanning Tunneling Microscopy III*" Springer-Verlag

[3] 西川　治：走査型プローブ顕微鏡　丸善　(1998)

[4] T.R. Albrecht, P. Grutter, D. Horne, D. Rugar: J. Appl. Phys. **69** (1991) 668.

[5] F. J. Giessibl: Science **267** (1995) 68.

[6] T. Uchihashi, Y. Sugawara, T. Tsukamoto, M. Ohta, S. Morita, M. Suzuki: Phys Rev. B**56** (1997) 9834.

[7] R. Perez, M.C. Payne, I. Stich, K. Terakura: Phys. Rev. Lett. **78** (1997) 678.

[8] I.Yu. Sokolov, G.S. Henderson, F.J. Wicks: Surf. Sci. **381** (1997) L558.

[9] F. J. Giessibl: Phys. Rev. B**56** (1997) 16010.

[10] N. Sasaki, M. Tsukada: Jpn. J. Appl. Phys. **37** (1998) L533.

[11] N. Sasaki, M. Tsukada: Jpn. J. Appl. Phys. **38** (1999) 192.

[12] M. Guggisberg, M. Bammerlin, R. Luthi, Ch. Lopparcher, F. Battiston, J. Lu, A. Baratoff, E. Meyer, H. -J. Guntherodt: Appl. Phys. A**66** (1998) S245.

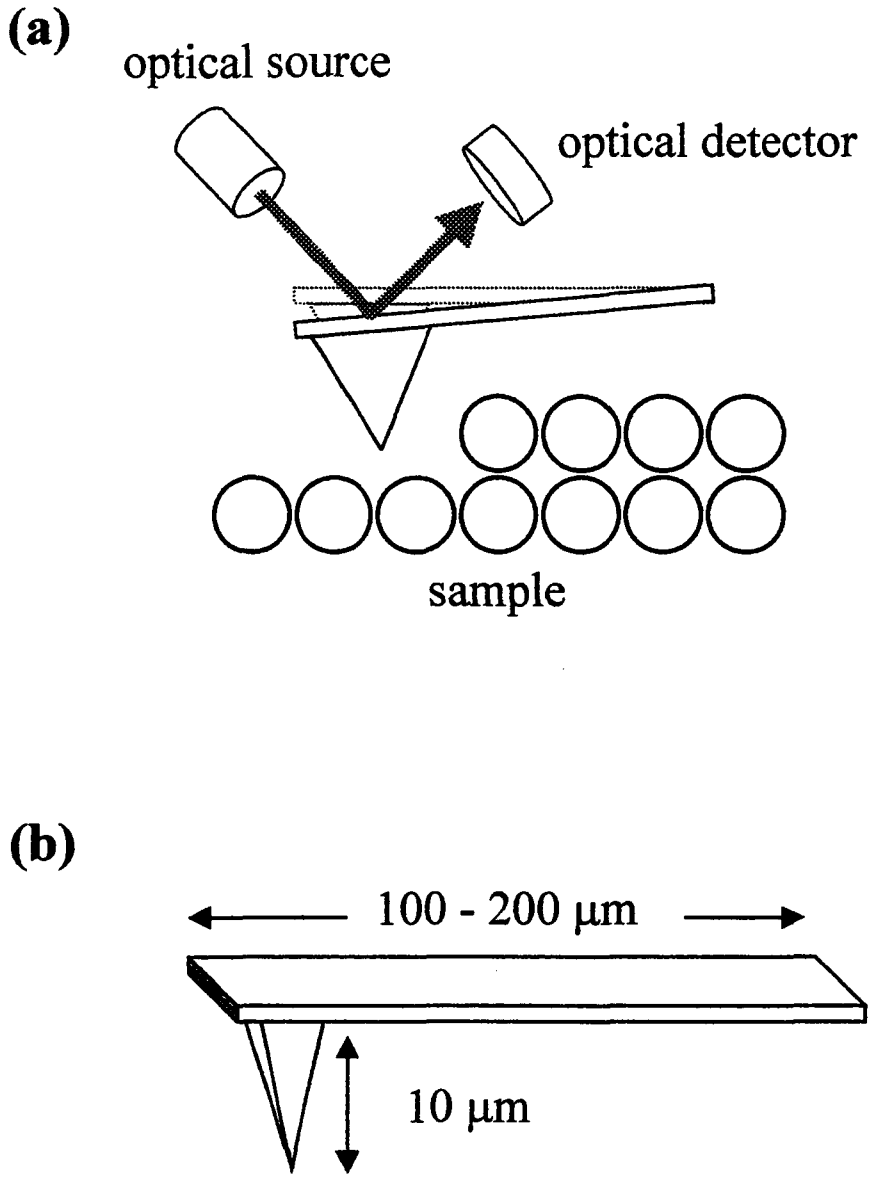

Fig. 2-1
The schematic illustration of (a) AFM and (b) a cantilever.

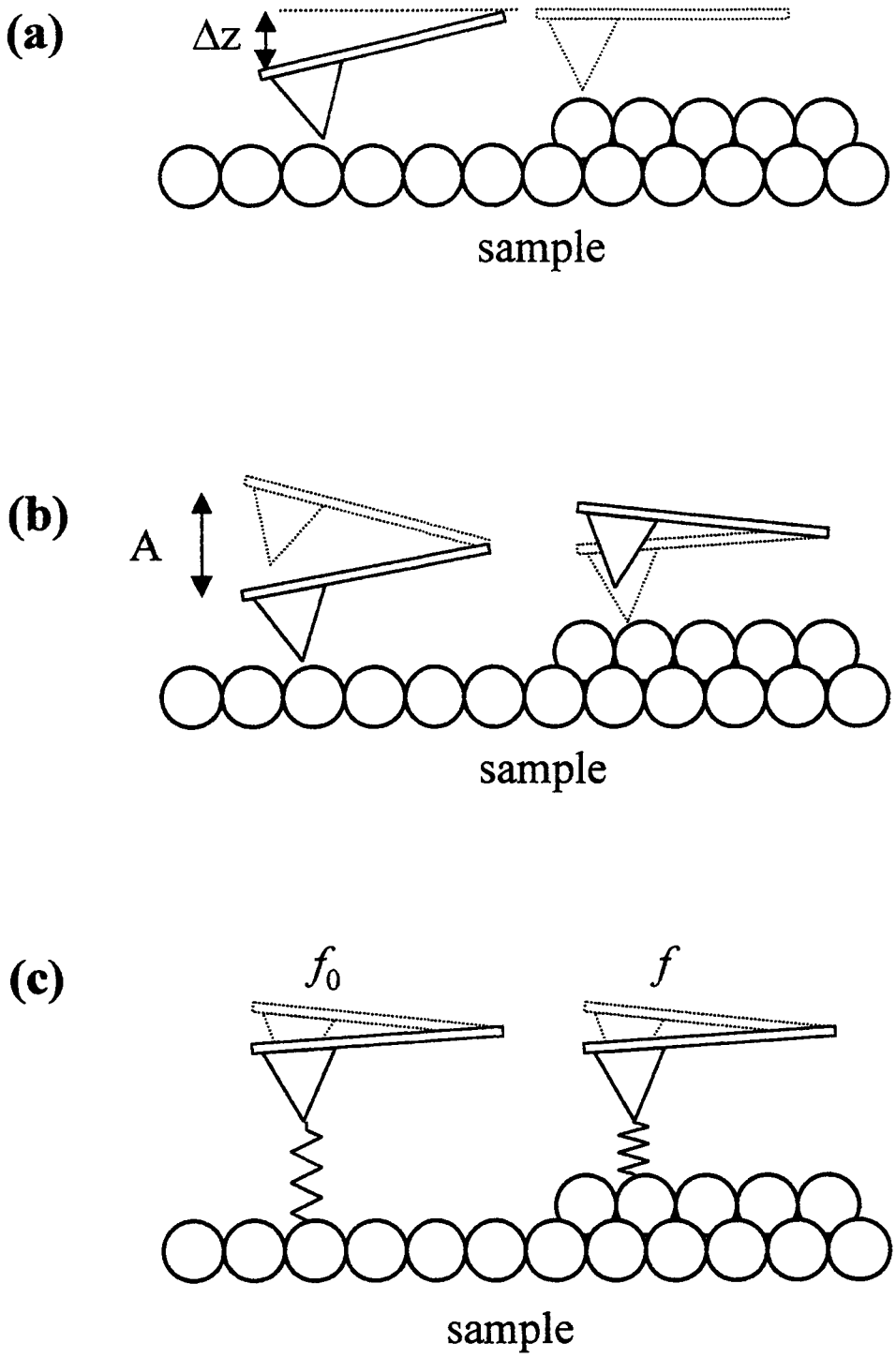

Fig. 2-2
Schematic illustration of AFM operation modes.
(a) Contact-mode. (b) Tapping-mode. (c) Noncontact.

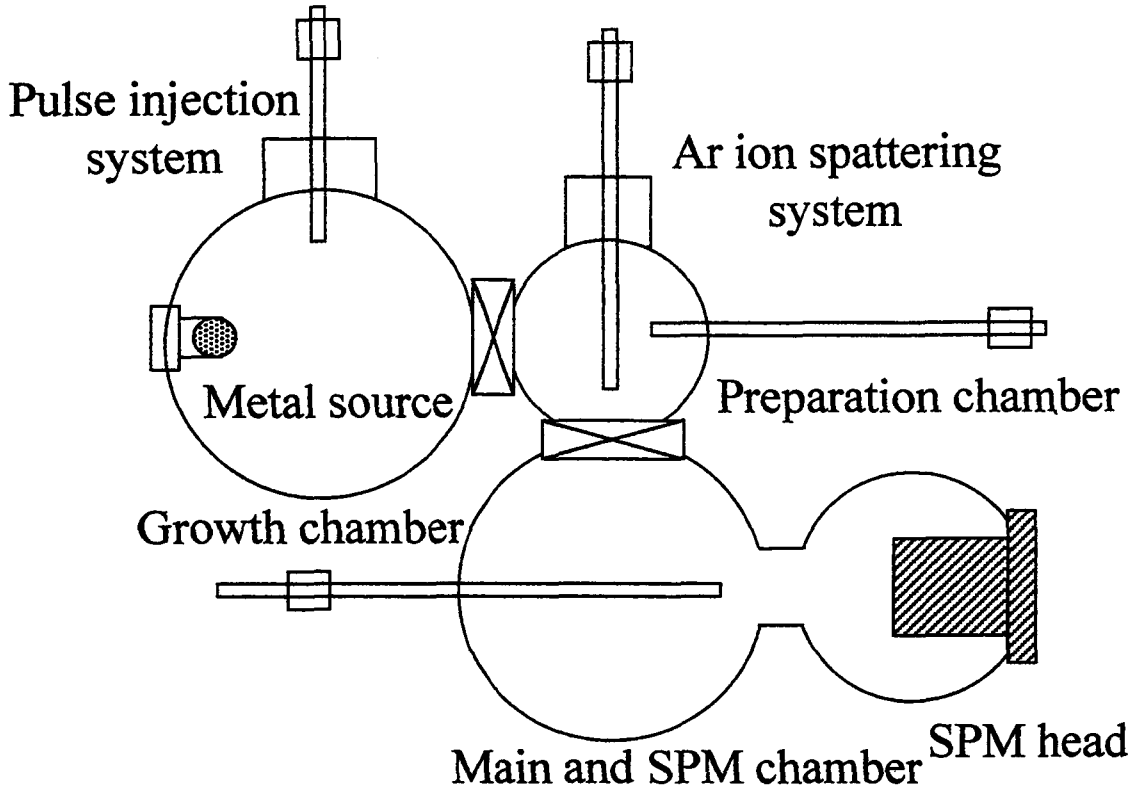

Fig. 2-3
Schematic illustration of the UHV system.

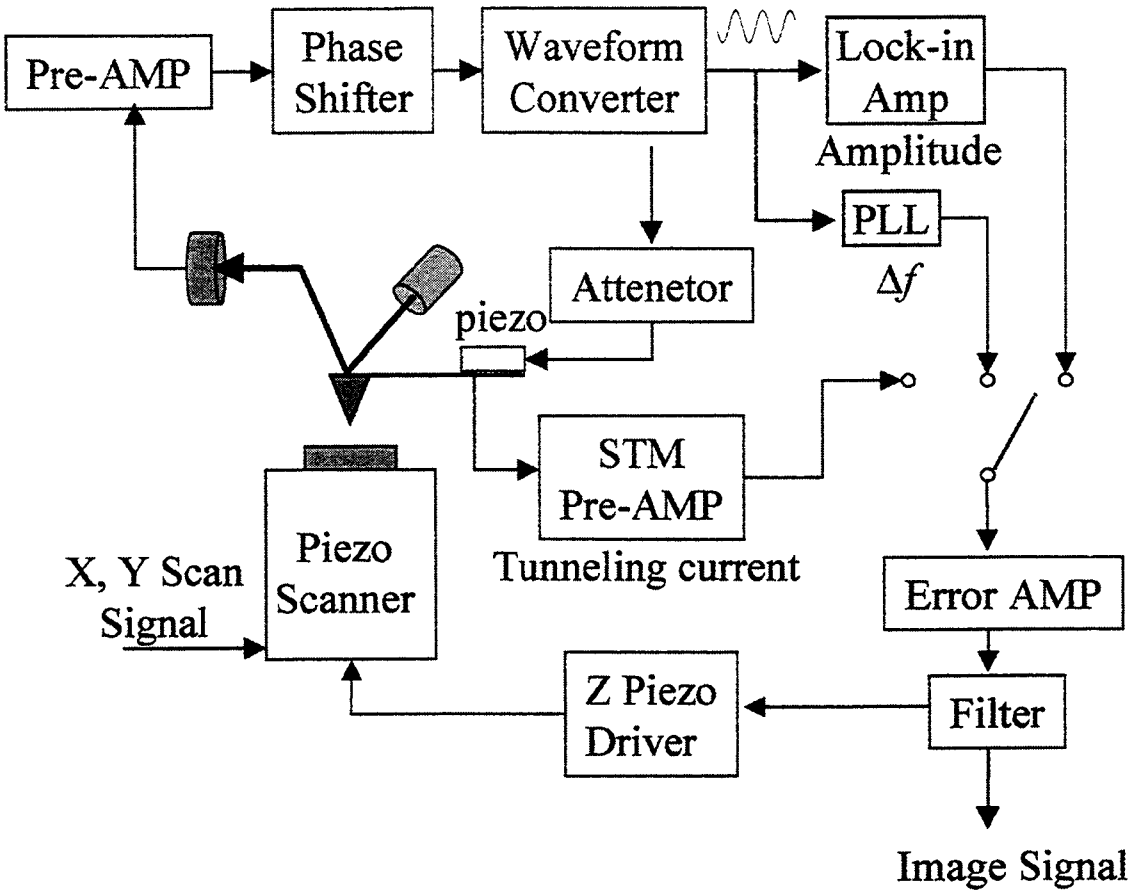

Fig. 2-4
Schematic diagram of NC-AFM/STM system.

Chapter 3

Noncontact AFM imaging of DNA molecules on mica surface

Chapter 3

NC-AFM imaging of DNA molecules on mica surface

3.1 Introduction

Mica surface is usually used for a substrate in conventional atomic force microscopy (AFM) observation of DNA [1-5]. DNA samples are prepared by wet process in air. Therefore, water and/or contamination layers are present on DNA samples [6]. This is quite different from well-defined surfaces which have observed by noncontact AFM (NC-AFM) [7-11].

In this chapter, NC-AFM observation of DNA molecules on mica surface is described. Force and frequency shift measurements revealed that water and/or contamination layer, which cause strong adhesion force, is present even under ultrahigh vacuum (UHV) condition. This measurement also revealed that electrostatic force makes large background force.

In spite of the presence of these long-range forces, single- and double-stranded DNA on mica were successfully observed by NC-AFM. The resolution of the images obtained by NC-AFM is higher than that of TM-AFM images. In addition, several NC-AFM images show contrast artifacts which might be useful for improving the resolution.

3.2 Experimental

Sample preparation

Single-stranded DNA (ssDNA) used was M13mp18 (from Takara Shuzo, 7250 bases) supplied at a concentration of 200 μg/ml in a solution of 10mM Tris-HCl and 1mM EDTA. In order to reduce its higher-ordered

structure, the ssDNA was denatured in 2% formaldehyde solution for 10 hours at room temperature. The final concentration of ssDNA was 20 μg/ml. Double-stranded DNA (dsDNA) used was pBluescript II KS(-) (from STRATEGENE, 2961 base pairs) supplied at a concentration of 1000 μg/ml. The dsDNA was diluted with water, and the final concentration of dsDNA was 10 μg/ml.

Freshly cleaved mica was used for a substrate to deposit DNA. To avoid substrate roughening, Mg(II) ion coating, which is usually used for controlling charge at the substrate, was not performed. The DNA was deposited on this substrate by placing a 1 μl drop of DNA solution on the substrate for several minutes. The solution was then removed by air-blowing. All samples were observed by NC-AFM in vacuum after TM-AFM observation in air.

NC-AFM imaging

NC-AFM observation was performed using an in-house UHV system equipped with a scanning probe microscope head (manufactured by JEOL). The DNA samples were loaded into the chamber and observed without or with preliminary treatments such as annealing. The rectangular Si cantilevers used had a spring constant of 30 N/m and a resonant frequency of 300 kHz. The cantilevers were used without any treatment. The tip-sample interaction was detected by frequency modulation (FM) detection as described in chapter 2. The frequency shift was used to control the tip-sample distance constant with constant oscillation energy.

TM-AFM imaging

To perform TM-AFM imaging in air, a conventional atomic force microscope (by Seiko Instruments) was used. The rectangular Si cantilever

used had a spring constant of 15 N/m and a resonant frequency of 135 kHz. The interaction between the tip and the sample was detected by amplitude modulation (AM) detection. All TM-AFM images were taken in constant amplitude mode, which provides a topographic image. The feedback amplitude was set to 70 % of the free-oscillation amplitude.

Frequency shift and force measurement

Frequency shift and force curve measurements were carried out using the same system used for NC-AFM observation. Three kinds of cantilevers were used: (1) rectangular undoped Si cantilevers with a spring constant of 15 N/m and a resonance frequency of 230 kHz; (2) rectangular doped Si cantilever (B doped, 0.002 Ωcm) having a spring constant of 15 N/m and a resonance frequency of 330 kHz; (3) tetragonal SiN cantilever having a spring constant of 0.09 N/m. The rectangular cantilevers were used for the frequency shift measurement and the tetragonal cantilevers were used for the force measurement.

3.3 Influence of adhesion and electrostatic force in NC-AFM

3.3.1 Adhesion force on mica surface

Figure 3-1 shows the force curves (force-distance curves) measured on a mica surface. In this figure, negative and positive values correspond to attractive and repulsive forces, respectively. The maximum attractive force shows an adhesion force between the tip and the sample. The adhesion force measured in air is about 10 nN as shown in Fig. 3-1(a). Figure 3-1(b) shows the force curve measured after the sample was left overnight in UHV at room temperature. The value of the adhesion force measured in UHV was

equal to that measured in air. Conversely, after the sample was annealed at 100 °C for 30 minutes, the adhesion force was half of the value measured in air, as shown in Fig. 3-1(c). This indicates that the annealing is necessary even in UHV to reduce the adhesion force which is caused by water and/or contamination layer on the mica surface.

3.3.2 Frequency shift

The electrostatic force is described as a function of surface potentials: $F \propto (V_{tip} - V_{sample})^2$

where V_{tip} and V_{sample} are potential of tip and surface, respectively. Fig. 3-2 shows a relationship between the tip bias voltage and the tip displacement measured on untreated mica surface. The frequency shift was set to 30 Hz. The curve shows the parabolic shape. The minimum value is obtained at -4 V. The minimum values do not occur at zero bias voltage implying the difference of surface potential between the tip and the sample.

The effects of sample annealing and tip bias appear in the relationship between frequency shift and distance as shown in Fig. 3-3. Curve 1 represents the measurement for an untreated mica surface without tip bias. Curve 2 shows the result for an untreated mica surface with tip bias of -3.5 V, which was chosen to minimize the difference of surface potentials. Curve 3 shows the result for an annealed mica surface with the bias of -2.0 V. These curves can be characterized by the slopes in region A and B which are related to long-range interaction (i.e., adhesion and electrostatic forces) and short-range interaction (i.e., van der Waals force), respectively. Curve 1 decreases slowly in region A, indicating presence of the electrostatic and/or adhesion forces. These interactions can be reduced by supplying tip bias voltage as curve 2 shows. The flat dependence in region A can only be

achieved by combining annealing the sample and supplying tip bias as shown in curve 3. This suggests that sample annealing and tip bias eliminate adhesion and electrostatic forces.

3.3.3 NC-AFM imaging

NC-AFM imaging was performed on mica surfaces to confirm influence of adhesion and electrostatic forces. Fig. 3-4 shows NC-AFM images of DNA on an untreated mica surface. Just after approaching a tip to the sample, DNA fragments were observed at a frequency shift of 15 Hz as shown in (a). At the second imaging, however, the fragments were not observed at a frequency shift of 15 Hz as shown in (b). The fragments were observed at a frequency shift of more than 50 Hz. An unclear rod like structure, which is not observed in (a), was observed in (b), suggesting that large long-range force, i.e. electrostatic force, is present. After annealing the sample, DNA molecules were stably observed at a frequency shift of 20 Hz as shown in Fig. 3-5. These results indicate that the surface is locally charged up under the presence of water and/or contamination layers, which disturb NC-AFM imaging.

Fig. 3-6 shows the results of controlling the electrostatic force by supplying tip bias voltage. In this experiment, the sample was annealed at 100 °C for 30 minutes. DNA molecules were observed with frequency shift of 23 Hz at tip bias voltage of -1.9 V which gives a minimum electrostatic force. Conversely, without bias voltage, DNA molecule was not observed with a frequency shift of 23 Hz. This result indicates that the electrostatic force can be reduced by supplying tip bias voltage.

3.4 High resolution imaging of single- and double-stranded DNA on mica surface

The samples in this experiment were not annealed to avoid thermal deterioration of DNA. This means that adhesion and electrostatic forces were present in all samples as mentioned above. When frequency shift is set to 100 Hz the tip probes mainly these long-range forces and the NC-AFM image shows weak contrast as shown in Fig 3-7(a). The clear contrast image as shown in Fig. 3-7(b) requires a frequency shift to be as large as the critical value of 150 Hz.

Figure 3-8(a) shows a topographic image of ssDNA taken by TM-AFM in air. Two strands can be seen in this image. Many kinks and nodes, which are caused by higher-ordered structure of ssDNA, can be observed. The height and width of the ssDNA are 0.6 and 15 nm, respectively, which are consistent with the data reported by Thundat et al [5]. Figure 3-8(b) shows the frequency-shift image of ssDNA taken by NC-AFM in vacuum conditions with a mean frequency shift of 120 Hz and free oscillation amplitude of 40 nm. During NC-AFM imaging, the oscillation amplitude was reduced to 50-80 % of the free oscillation amplitude. This image also reveals many kinks and nodes and a width of 10 nm, which is almost the same as the TM-AFM image. However, the magnified image in Figure 3-8(c) reveals a coiling structure with a resolution of 3 nm which cannot be observed by TM-AFM.

The difference in resolution between TM- and NC-AFM was also observed for dsDNA. Figure 3-9(a) shows the topographic image of dsDNA taken by TM-AFM in air. In this image, two DNA strands can be seen. Its height and width are 0.7 nm and 20 nm, respectively. The DNA strands are

piled up at the center of the image. At this point, height of the DNA is 1 nm, which is 0.3 nm larger than that of other points. However, each DNA strand can barely be discerned. Figures 3-9(b) and (c) show the frequency-shift images taken by NC-AFM with a mean frequency shift of 130 Hz and free oscillation amplitude of 20 nm. In Fig. 3-9(b), two dsDNA strands can be seen and the width of the dsDNA is 10 nm. This value is half of the value in TM-AFM. The dsDNA strands have many nodes and are twisted together at the point indicated by the arrow. This twisted structure can be clearly seen in the magnified image as shown in Fig. 3-9(c). Two DNA strands are separated at the upper-left and the lower-right sides of this image and are twisted at the center of the image.

Figure 3-10 shows the magnified image of Fig 3-9(b) and the sectional profile along the dsDNA strand. In Fig. 3-10(a), DNA's structures on the right and left side of a kink, which is shown at the center of this image, are quite different. On the right side, the DNA molecule shows a helix structure and the strands are separated at both end. The pitch length of the helix structure is 6-8 nm as shown in Fig. 3-10(b). This value is 2 times as large as that of Watson-Crick model, indicating deformation of double helix structure. On the left hand, the DNA molecule has some nodes, but the double helix structure can not be seen. This suggests that the DNA keep the Watson-Crick double helix structure on this side.

The NC-AFM images of ssDNA and dsDNA reveal detailed structures which cannot be seen in the TM-AFM images. There are two possibilities to explain this difference. One is a structural change caused by the atmosphere presence during measurement. The TM-AFM imaging was performed in air, which contains a large proportion of water. In contrast, the NC-AFM

imaging was performed in vacuum, which is a totally dry environment. If the DNA structures become looser under such dry conditions, thereby increasing their degree of contact with the substrate, they would then be easier to observe in vacuum than in air.

Another possibility is the difference in resolution between NC-AFM and TM-AFM. In both operating modes, the widths of the DNA images are almost equal (~10 nm). Since the actual width of a DNA molecule is 2 nm, the observed width would reflect only the tip radius (~10 nm) in both modes. However, NC-AFM is more highly sensitive to the interaction between the tip and the sample than TM-AFM, resulting in a high-contrast resolution in terms of the gray-scale. A possible mechanism of the NC- and TM-AFM is schematically illustrated in Figure 3-11. Assuming that the tip is composed of a bulk-tip having a 10 nm diameter and a nano-tip located at the top of the bulk-tip, these contribute to a NC-AFM imaging. In each case of NC- and TM-AFM imaging, the bulk tip forms the outline of the DNA molecule. The width of the outline related to the bulk tip radius (~10 nm). In the case of NC-AFM imaging, the nano-tip can trace the detailed structure because the extremely high sensitivity of NC-AFM prevents the deformation of the mini-tip (Fig. 3-11(a)). As a result, NC-AFM is able to reveal detailed features in the outline of the DNA strands.

This high-contrast resolution causes the contrast artifacts which often appear depending on the oscillation amplitude and/or feedback conditions. Figure 3-12(a) shows a topographic image of ssDNA taken by NC-AFM. The contrast of this image is reversed and the edges on the both sides of the ssDNA are enhanced. Considering the actual width of DNA, the separation between these edges might be due to the tip radius. Figure 3-12(b) shows an

image of aggregated ssDNA strands. In this image, the sharp lines and folded structure can be clearly seen. The origin of these contrast artifacts is currently unclear. However, they might provide information on the detailed structure, suggesting the possibility of improving the resolution of NC-AFM.

3.5 Conclusion

We have successfully imaged single- and double-stranded DNA adsorbed on mica substrate by NC-AFM in vacuum. Despite the existence of strong adhesion and/or electrostatic forces, high-resolution DNA images were obtained by NC-AFM. NC-AFM images reveal the detailed structures, including the coiling structure of single-stranded DNA and the helix structure of double-stranded DNA, which are not revealed by TM-AFM.

Several NC-AFM images have contrast artifacts which might provide information of detailed structures. These results suggest the possibility of improving resolution of NC-AFM images even further, which is an encouraging step toward directly observing the double helix and analyzing the base sequence of DNA.

3.6 References

[1] H. G. Hansma, I. Revenko, K. Kim, D. E. Laney, Nucleic Acids Res. 24 (1996) 713.

[2] H. G. Hansma, D. E. Laney, M. Bezanilla, R. L. Sinsheimer, Biophysical J. 68 (1995) 1672.

[3] H. G. Hansma, R. L. Sinsheimer, J. Groppe, T. C. Bruice, V. Elings, G. Gurley, M. Bezanilla, I. A. Mastrangelo, P. V. C. Hough, P. K. Hansma, Scanning 15 (1993) 296.

[4] T. Thundat, D. P. Allison, R. J. Warmack, J. Vac. Sci. Technol. A 11 (1993) 824.

[5] T. Tundat, D.P Allison, R.J. Warmack, G.M. Brown, K.B. Jacobson, J.J. Schrick, T.L. Ferrell: Scanning Microscopy 6 (1992) 911

[6] Y. Sugawara, M. Ohta, T. Konishi, S. Morita, M. Suzuki, Y. Enomoto: Wear 168 (1993) 13

[7] F. J. Giessibl, Science, 267 (1995) 68.

[8] T. Uchihashi, Y. Sugawara, T. Tsukamoto, M. Ohta, S. Morita, Phys. Rev. B 56 (1997) 56.

[9] K. Fukui, H. Onishi, Y. Iwasawa, Phys. Rev. Lett. 79 (1997) 4202.

[10] S. Kitamura, M. Iwatsuki, Jpn. J. App. Phys. 35 (1996) 668.

[11] Y. Sugawara, M. Ohta, H. Ueyama, S. Morita, Science 270 (1995) 1646.

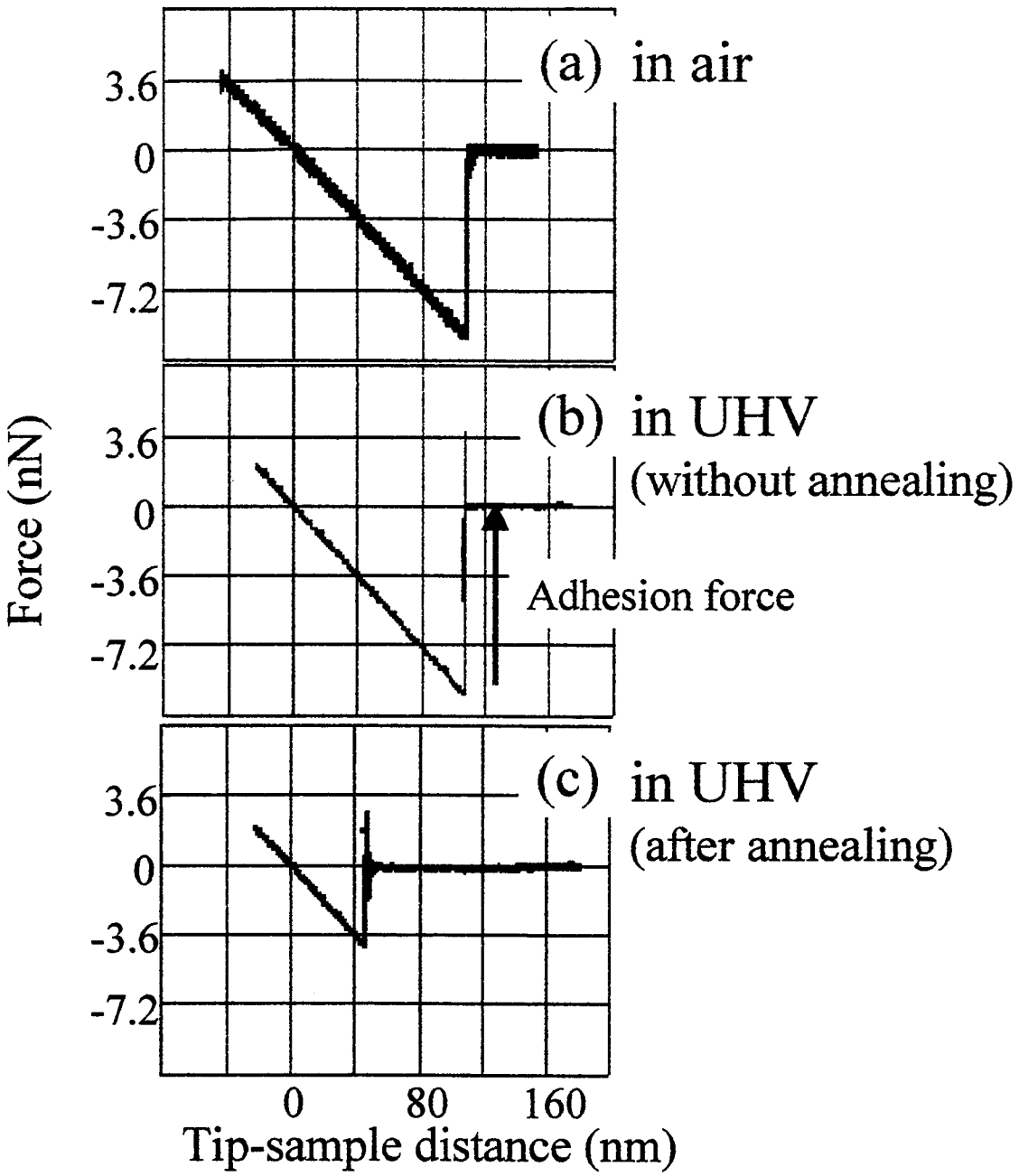

Fig. 3-1
Force-distance curves measured on a mica surface.

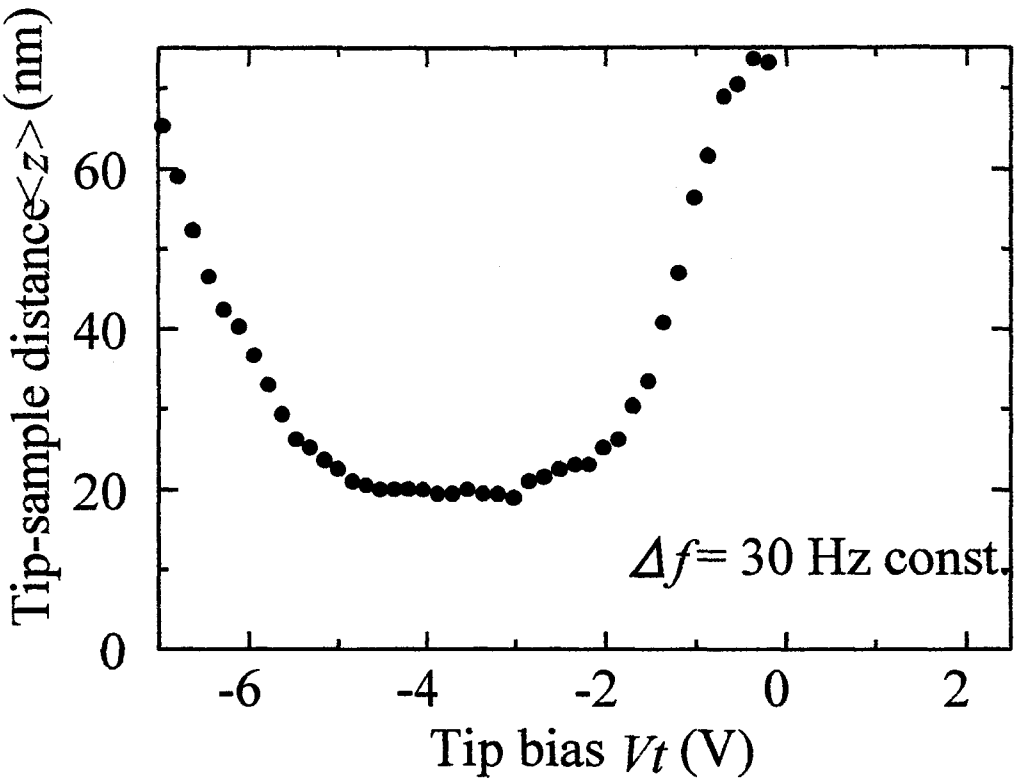

Fig. 3-2
Tip bias dependence of tip-sample distance. The measurement was performed at frequency shift of 30 Hz.

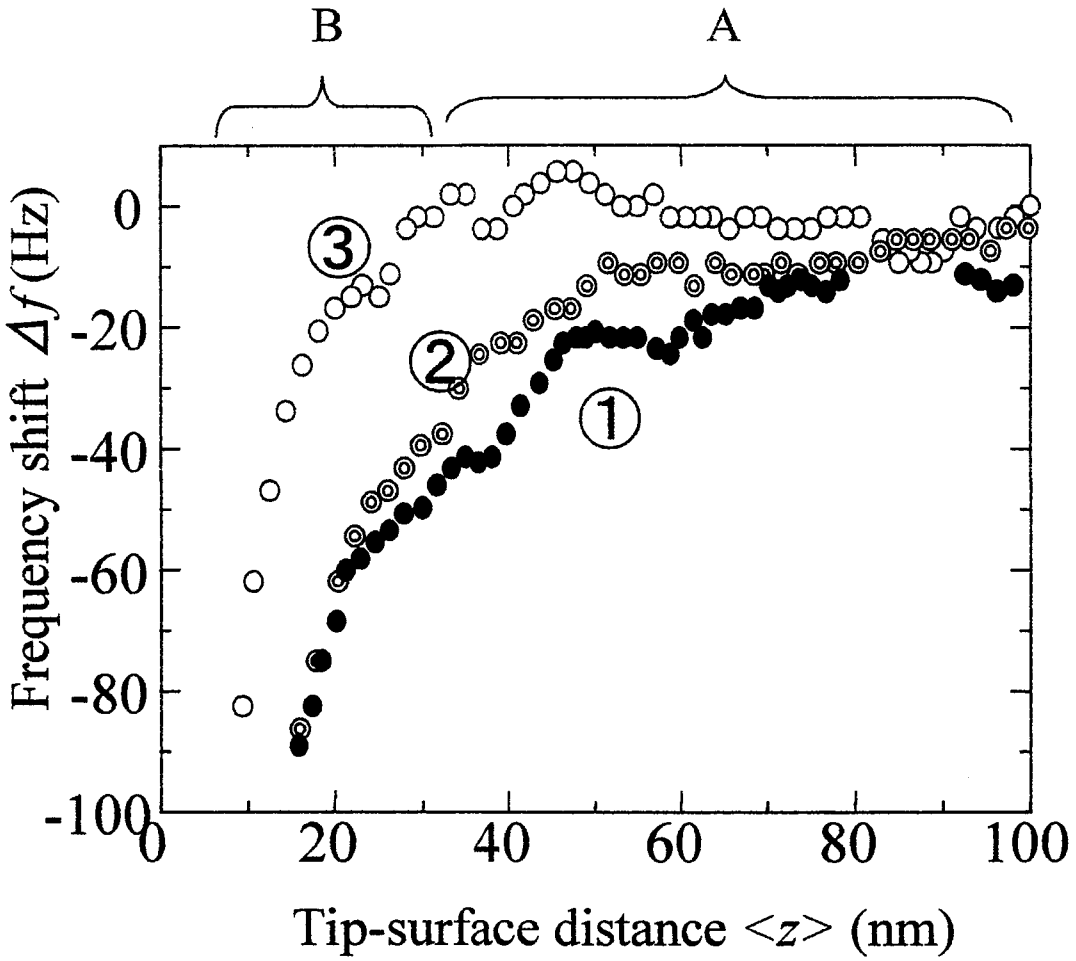

Fig. 3-3
Variation of frequency shift as a function of the tip-sample distance. These curves were obtained (1) at tip bias of 0 V for an untreated mica, (2) at tip bias of -3.5 V for an untreated mica and (3) at tip bias of -2 V for an annealed mica.

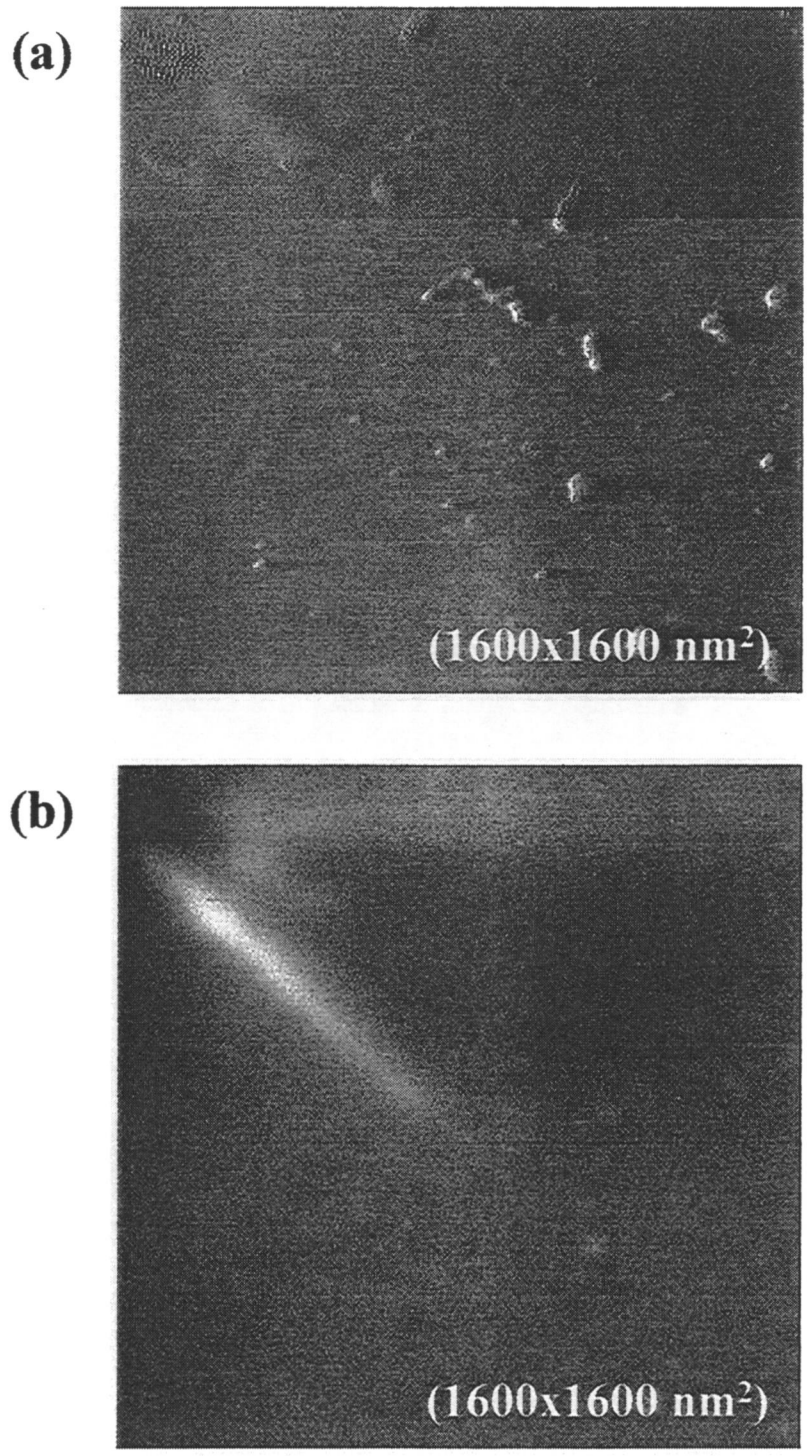

Fig. 3-4
NC-AFM images obtained on an untreated sample at of frequency shift of 15 Hz. (a) The first scan and (b) the second scan after approaching the tip to sample.

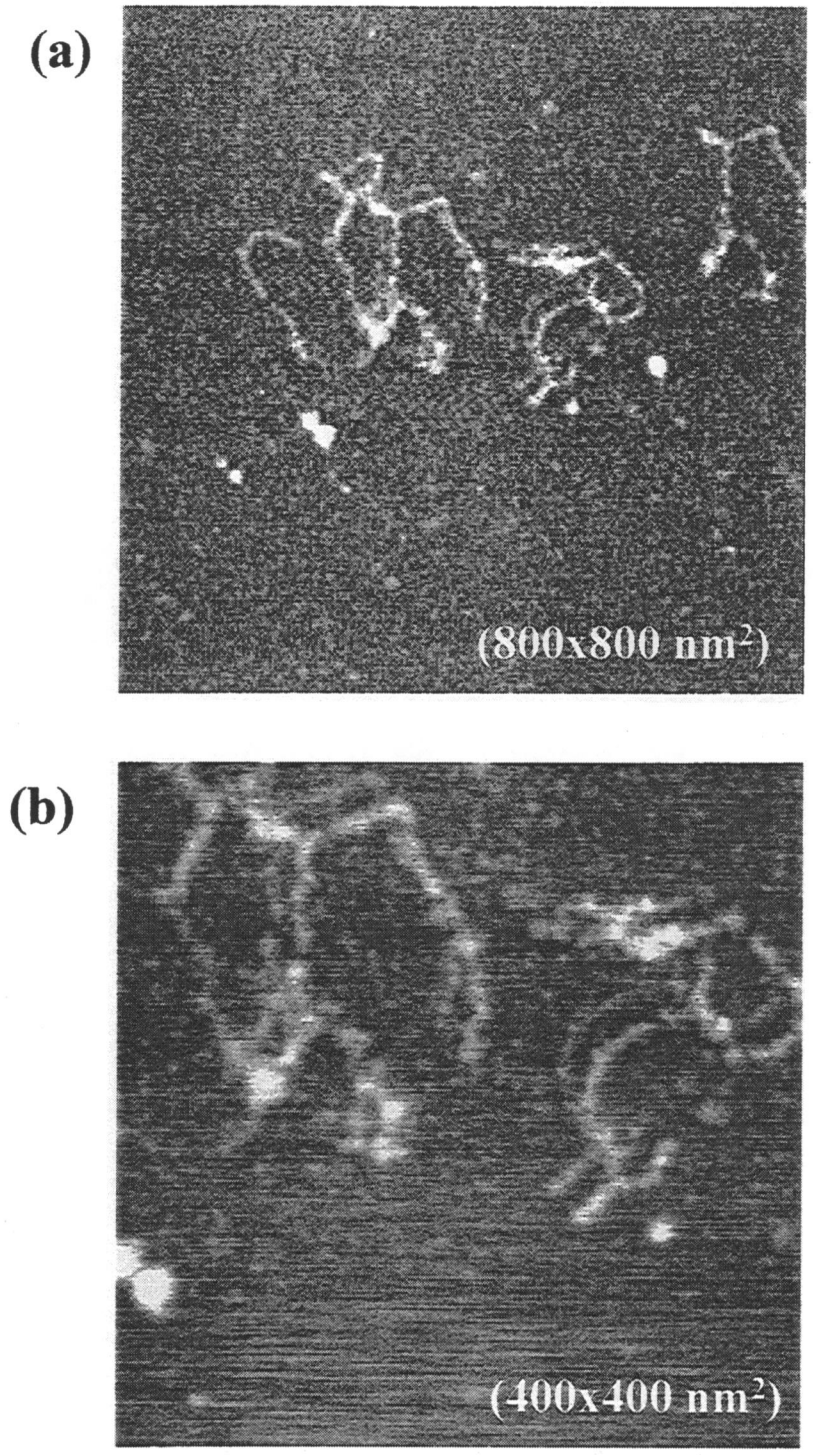

Fig. 3-5
NC-AFM images obtained on annealed sample at frequency shift of 20 Hz. (a) The first and (b) the second scan after approaching the tip to sample.

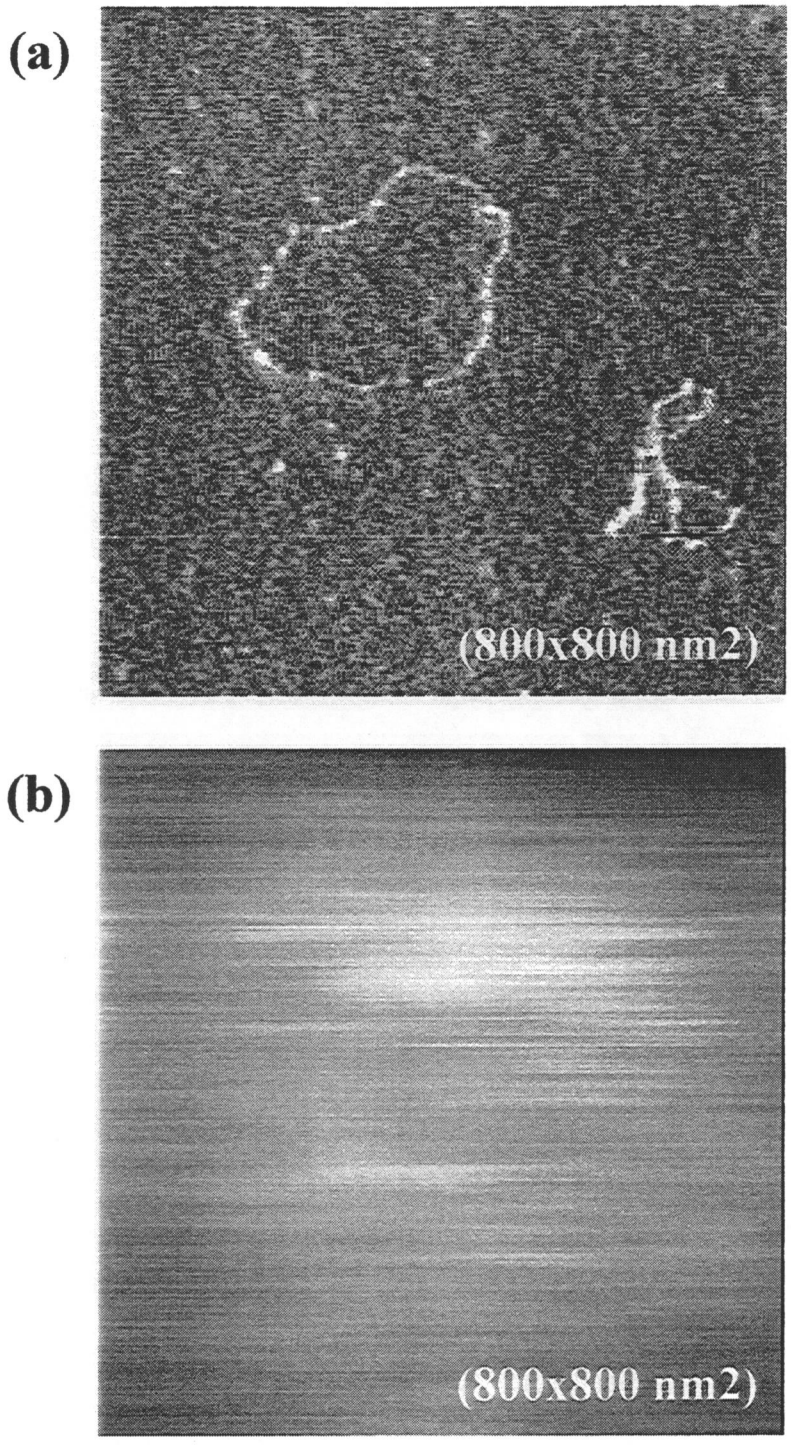

Fig. 3-6
NC-AFM images obtained after annealing the sample with (a) tip bias voltage of -1.9 V and (b) 0 V. The frequency shift was 23 Hz.

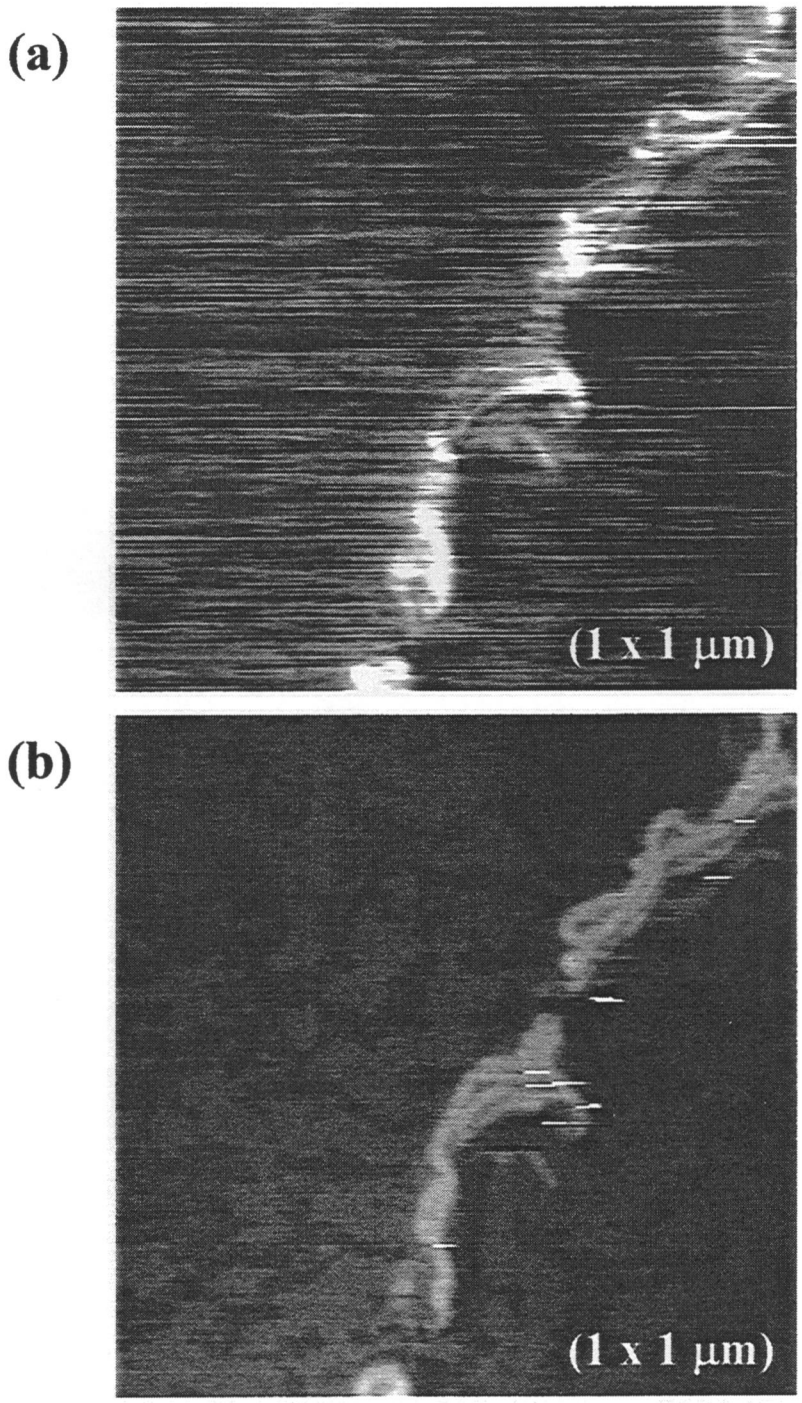

Fig. 3-7
NC-AFM images of aggregated single-stranded DNA obtained at frequency shift of (a) 100 Hz and (b) 150 Hz.

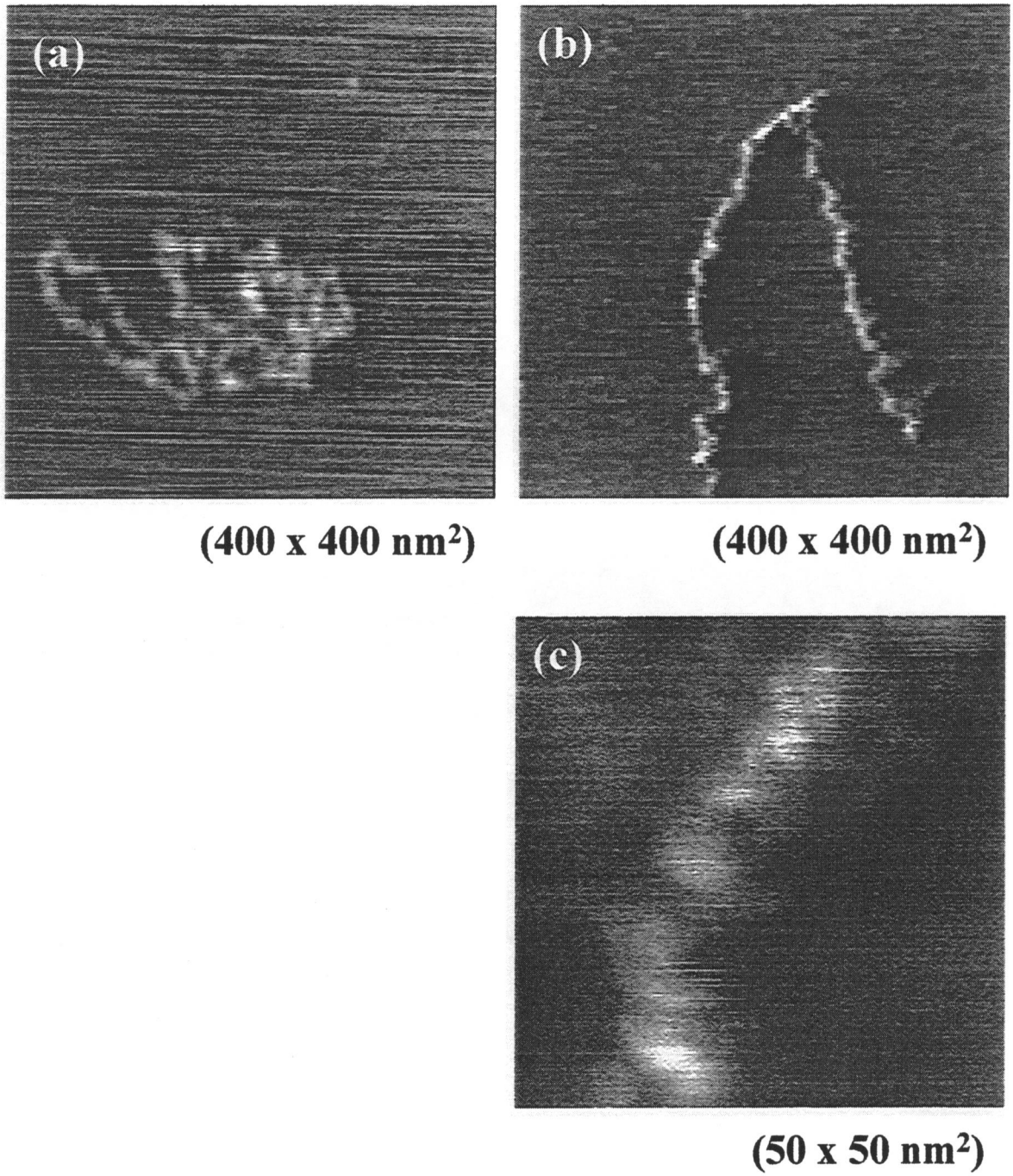

Fig. 3-8
Single-stranded DNA images observed by TM-AFM and NC-AFM: (a) Topographic image taken by TM-AFM. (b) Frequency shift image taken by NC-AFM. (c) A magnified image of (b).

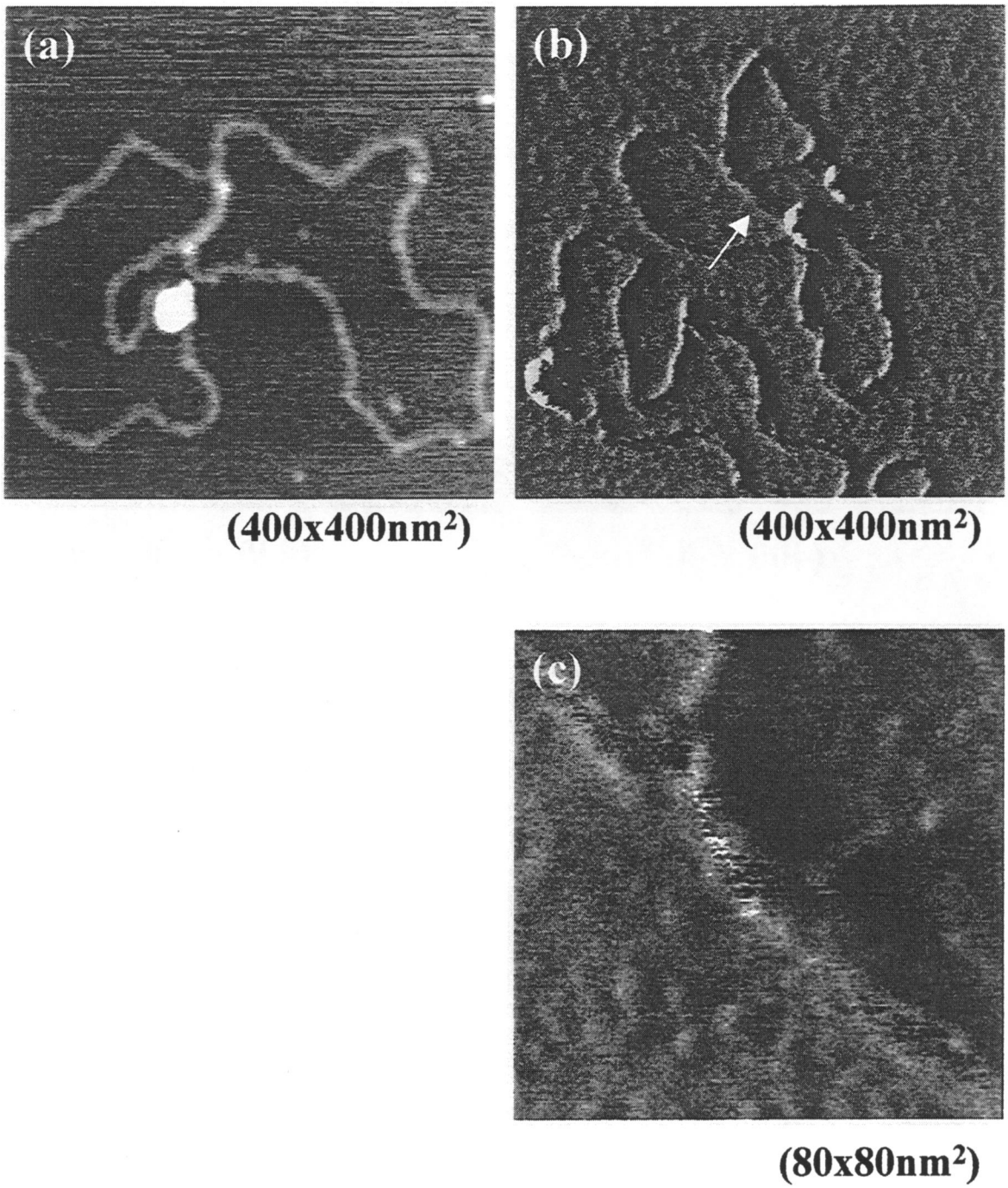

Fig. 3-9
Double-stranded DNA images observed by TM-AFM and NC-AFM: (a) Topographic image taken by TM-AFM. (b) Frequency shift image taken by NC-AFM. (c) A magnified image of (b).

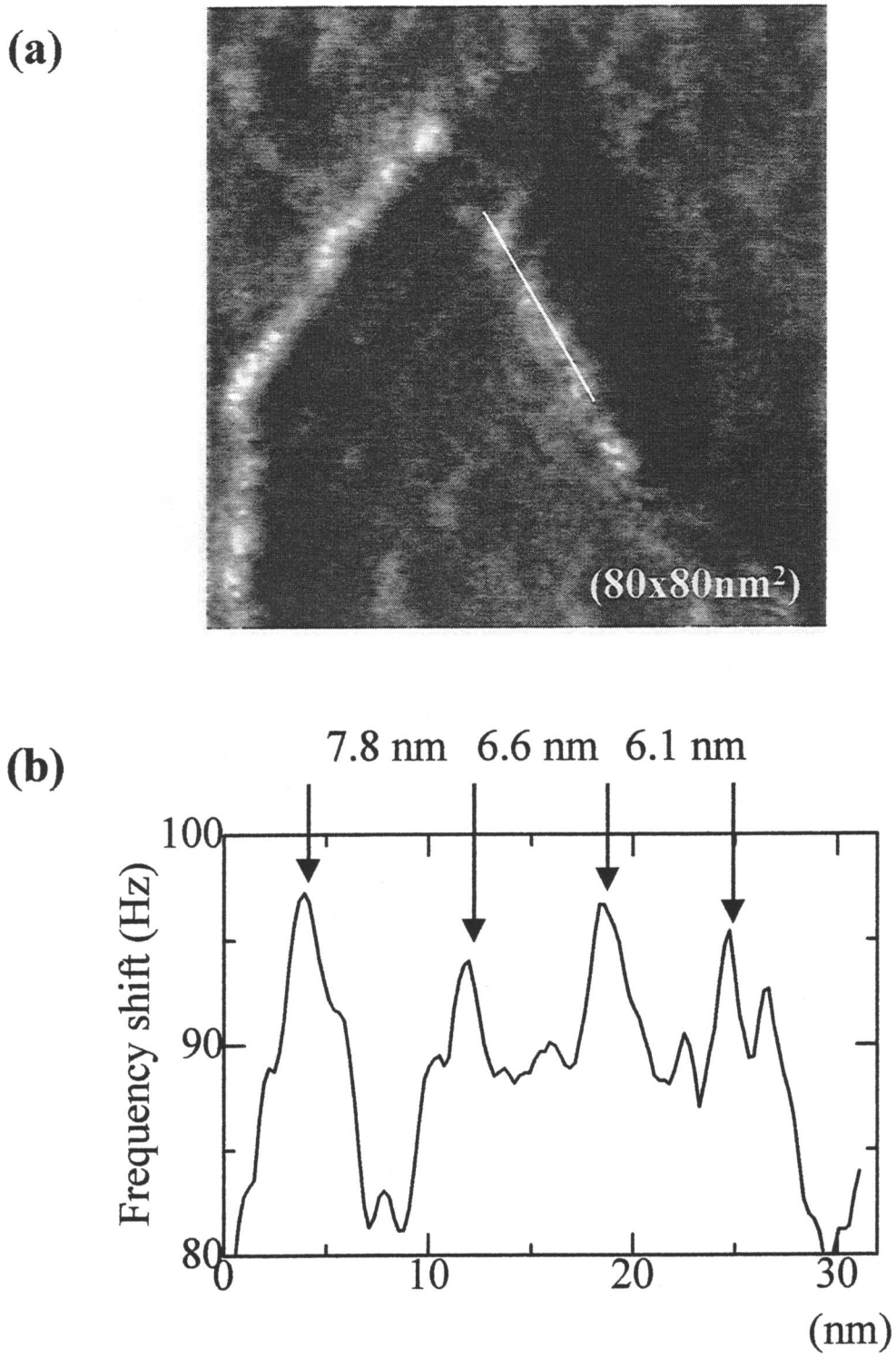

Fig. 3-10
(a) Double-stranded DNA image observed by NC-AFM.
(b) Sectional profiles of (a) along the line.

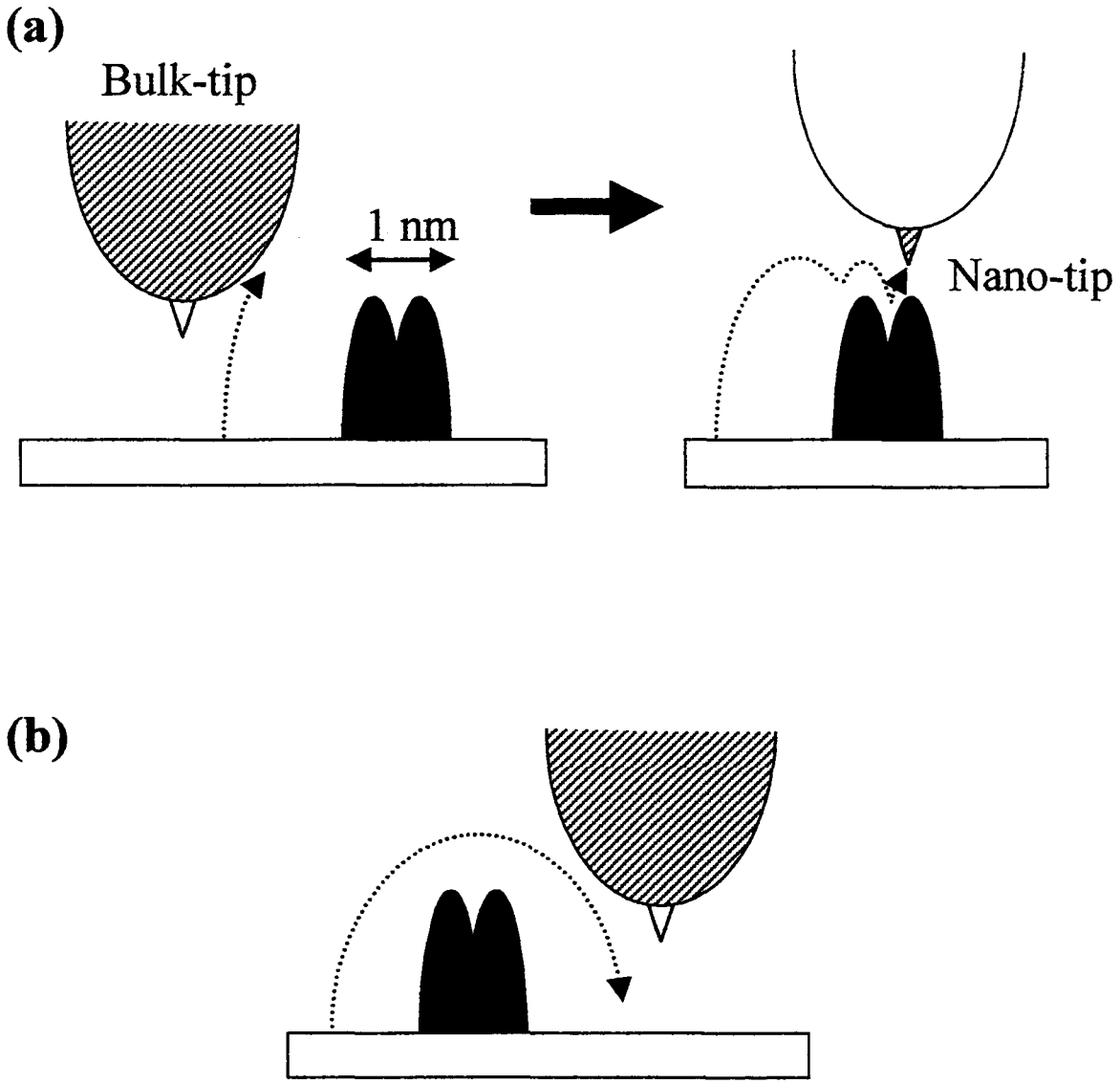

Fig. 3-11
Schematic illustration for possible mechanism of contrast artifact. (a) Both mesoscopic and nano tip are able to contribute to NC-AFM images. (b) Nano-tip is not active for imaging in TM-AFM.

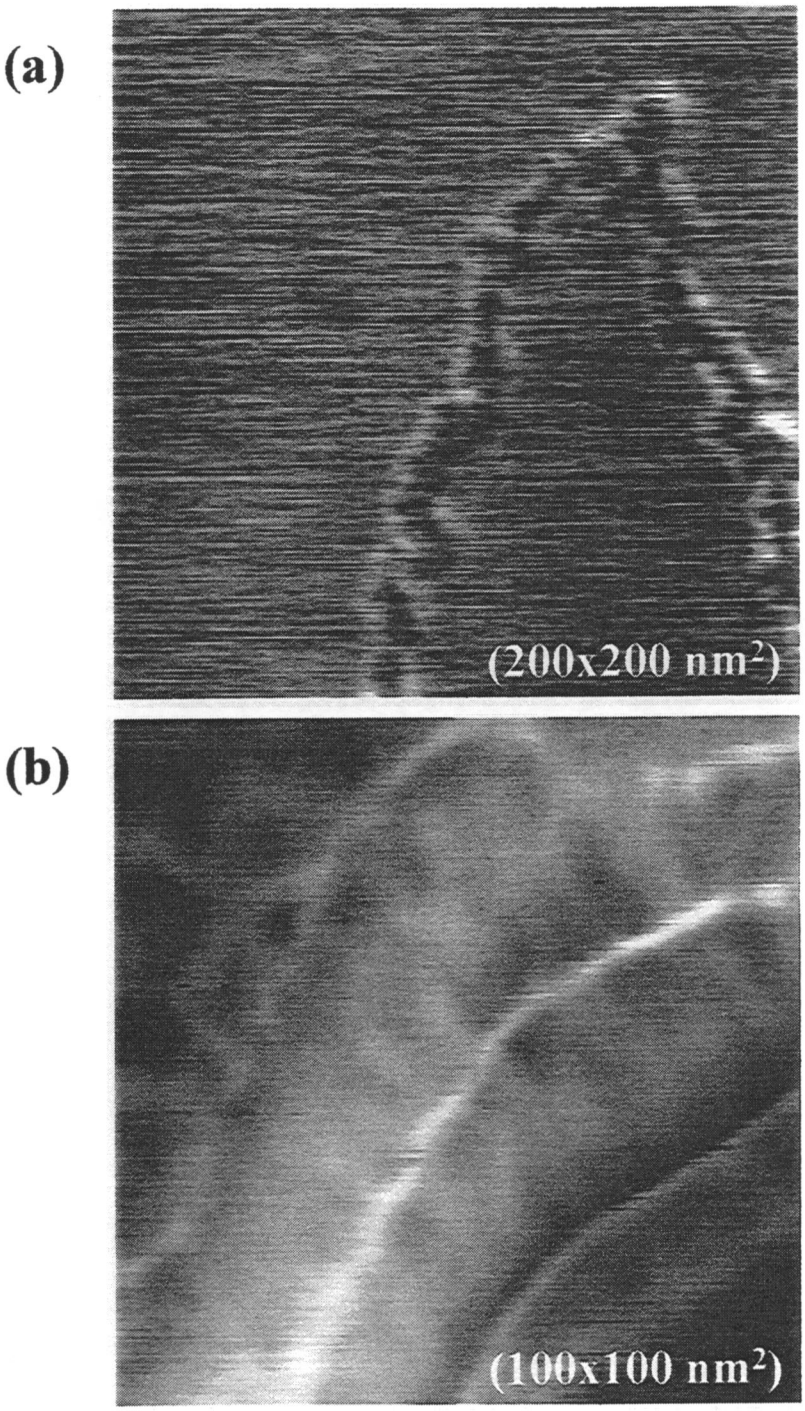

Fig. 3-12
Contrast artifact in single-stranded DNA images taken by NC-AFM. Image (a) shows the reversed contrast and edge enhancement on a DNA image and image (b) shows the sharp lines and folded structures.

Chapter 4

Imaging of double helix structure on Cu(111) surface

Chapter 4

Imaging of double helix structure on Cu(111) surface

4.1 Introduction

As described in chapter 3, single- and double-stranded DNA have been successfully observed by NC-AFM in spite of the presence of the strong adhesion and electrostatic forces. The observed NC-AFM images had higher resolution than that of TM-AFM images. This shows that current resolution limits mainly arise from difficulty of controlling a tip shape.

Because of high topological protrusion of DNA molecules, high aspect ratio and small apex radius is required for high-resolution imaging of DNA molecules. Supplying high bias voltage induces migration of tip and/or surface atoms. This allows us to control the tip shape [1]. In this chapter, NC-AFM observation on Cu(111) surface using shape-controlled tip to observe double helix of DNA is described. The NC-AFM images revealed the DNA double helix structure that has not been observed using AFM to date.

4.2 Experimental

The circular double-stranded DNA used was pBluescript II KS(-) (STRATEGENE, 2961 base pairs) supplied at a concentration of 1000 μg/ml. It was diluted with water to produce a final concentration of 10 μg/ml. The DNA molecules were deposited on Cu(111) surface using pulse injection method [2-4]. Fig. 4-1 shows a schematic illustration of the pulse injection method. The substrate was set below the pulse valve and the

distance between the substrate and the valve was about 13 cm. This system was equipped with the evaporation chamber (see chapter 2). About 100 μl of the solution was injected. This changed pressure form 10^{-8} to 10^{-3} Torr. After deposition, the sample was transferred to SPM head.

Rectangular Si cantilevers (silicon-MDT) were used which had a spring constant of 14 N/m and a resonant frequency of 300 kHz. The cantilevers were highly doped with boron and their specific resistance was 0.002 Ωcm. Fig. 4-2 shows the schematic diagram of NC-AFM. Deflection a cantilever was detected by optical reflection method. The cantilever was kept oscillating at its resonant frequency by applying positive feedback with constant excitation energy. The oscillation signal was put into the two-phase lock-in amplifier to detect the oscillation amplitude and put into the phase-locked loop circuit to detect frequency shift. The oscillation amplitude was used for feedback to keep the tip-sample distance constant, i.e. constant-amplitude mode. This mode is more stable than constant-frequency-shift mode for scanning DNA samples, which may include unavoidably large particles. Particles ranging from 4 to 6 nm height could be traced in constant-amplitude mode but not in constant-frequency-shift mode. The oscillation amplitude was set to 90% of the free oscillation amplitude for imaging. The mean frequency shift was 100–200 Hz.

4.3 Results and discussion

4.3.1 Cu(111) surface

The substrate used was a Cu(111) thin film deposited on cleaved mica surface. The Cu(111) thin film was fabricated in growth chamber whose base pressure is 10^{-8} Torr (see chapter 2). Before deposition, the mica

substrate was annealed for outgassing at 250 °C for 20 min. Cu was evaporated for 9 min with deposition rate of 0.1 nm/s and substrate temperature of about 200 °C. Then the Cu thin film annealed at 600 °C for 2 min. Fig. 4-3 shows (a) a STM image and (b) a sectional profile of the Cu(111) surface observed at sample voltage of -1 V and tunneling current of 0.1 nA. Steps can be seen in (a). Its height is 0.2 nm, which is consistent with single atomic-step height.

4.3.2 Pulse injection method

On the metal surface, aqueous solution forms a spherical shape because of hydrophobic property of metal surface. In such case, solute is dispersed toward edge of a drop by capillary flow [5]. Fig. 4-4 shows TM-AFM images of DNA deposited on Au surface by dropping and drying DNA solution (drop-and-dry method). At the edge of the drop, DNA formed a network structure whose height is 2-5 nm as shown in (a). At the center of the drop, there were many particles and DNA can not be observed as shown in (b). These results indicate that this method is not suitable to deposit DNA molecules on metal surface.

Fig. 4-5 shows NC-AFM images of DNA molecules deposited on (a) mica and (b) Au surface by the drop-and-dry method and Au surface by the pulse injection method. Isolated DNA molecules were observed in (a) and (c). On the other hand, DNA molecules were aggregated as shown in (b). These results indicate that the pulse injection method is useful to deposit DNA molecule on metal surface.

4.3.3 Tip treatment

Following procedure was used to improve a tip showing in Fig. 4-6. First, SiO_2 layer, which is formed naturally on a tip surface, was removed

by pushing the tip onto a surface with a load of 0.1–1.0 μN. The bare Si surface then appeared on the tip surface. Subsequently, high voltage was applied between the tip and the sample to form a needle-shaped tip. In this process, tip-sample distance was kept with the tunneling current without cantilever's oscillation. The supplied voltage was +/-10 V. Fig 4-7 shows tunneling current spectra measured on Cu(111) surface with conductive cantilever. Tunneling current is rectified before supplying high bias, indicating the presence of schottky barrier. This barrier can be eliminated by supplying high bias as shown in (b). The detailed procedure and mechanism of formation of the needle-shaped tip has been previously reported by Heike et al [1].

4.3.4 Imaging of double helix structure by NC-AFM

Fig. 4-8 shows NC-AFM images and a sectional profiles of double-stranded DNA on Cu(111) observed by NC-AFM (a) before and (b) after the tip-sharpening process. In (a), DNA molecules can be seen at the center of the image. The DNA can be seen to have a width of 7 nm which is much greater than the diameter of actual DNA and almost equal to the value obtained by TM-AFM in air. For this reason, this value merely reflects the tip radius. After the tip was sharpened, the resolution improved dramatically as shown in Fig. 4-8(b). The steps and triangular terraces of the Cu(111) surface can be clearly seen. The observed step height of Cu(111) is 0.2 nm, which agrees closely with a height of single atomic step of Cu(111). In this image, a partially crossed double-stranded DNA molecule about 4 nm wide can also be observed. The width suggests that resolution of the image is significantly improved in comparison with previously reported DNA images by AFM in any scan mode. Such extreme change in resolution is unusual in

Table 1
Height of double-stranded DNA observed by NC-AFM (constant frequency-shift mode and constant amplitude mode) in vacuum and TM-AFM in air. The substrates used were Cu(111) and mica.

		force	Cu(111)	mica
NC-AFM (in vacuum)	constant frequency-shift	0.05-0.4 nN attractive	0.3-0.6 nm	
	constant amplitude	≪1nN repulsive	0.6-0.8 nm	~1 nm
TM-AFM (in air)		1-10 nN repulsive		~0.8 nm

any AFM operating mode except for NC-AFM. A possible mechanism for this sudden change is illustrated in Fig. 4-9. Assuming that the nano-tip is formed using the tip-improvement procedure mentioned above, this nano-tip can only be used in noncontact mode as the extremely high sensitivity of NC-AFM prevents deformation of the nano-tip.

Fig. 4-10 shows high-resolution images of the DNA molecule. Periodic corrugation along the DNA molecules is observed in Fig 4-10(a). This image differs significantly from featureless DNA images previously obtained by tapping-mode AFM in air. The repeat distance of this periodic structure is 3–5 nm as shown in Fig 4-10(b). This value agrees with the periodicity of Watson-Crick model, indicating that the double helix structure was successfully observed by NC-AFM. Fig. 4-11(a) shows the distribution of the pitch lengths of the double helix structure observed in Fig. 4-10. The most frequently value is 3.5-4.0 nm reflecting the Watson-Crick double helix structure. However, the pitch lengths were widely distributed in the range of 2-7 nm.

Table 2
The structure of double-stranded DNA observed by NC-AFM and Watson-Crick model.

	NC-AFM	Watson-Crick model
Height	0.6-0.8 nm	2 nm
Pitch length	2-4 nm (3-4 nm)	3.4 nm
Width	4 nm	2 nm

Conversely, the observed height of the DNA molecule is ~1 nm which is obviously lower than that of Watson-Crick model (2 nm). Table 1 shows heights of DNA molecules observed on Cu(111) and mica surfaces using amplitude and frequency-shift mode of NC-AFM in vacuum and TM-AFM in air. Typical tip-sample interactions in frequency-shift mode of NC-AFM and TM-AFM have been estimated as attractive force of 0.05-0.1 nN [6-9] and repulsive force of 1-10nN [10], respectively. The interaction in amplitude mode is supposed to be middle of these interactions. In spite of such difference of the tip-sample interactions, the DNA heights were observed as 0.5-1 nm. This indicates that tip-sample interactions in NC-AFM observation do not deform DNA molecule, and the height of DNA on surfaces is actually 1 nm.

The observed DNA structure is compared with Watson-Crick model in Table 2. Most frequently value of observed pitch length is 3.5-4.0 nm which is consistent with the Watson-Crick model. However, the height is half of the value of Watson-Crick model and the pitch lengths are widely distributed. These results suggest that the double helix structure was deformed on Cu(111) surface.

There are two possibilities for the deformation of DNA molecules. One is deformation on surface. Double helix structure is mainly formed by hydrogen bonding and hydrophobic interaction between nucleic acid bases. Especially, hydrophobic interaction is important to stabilize the double helix structure. This interaction, however, disappears in vacuum which is totally dry environment. In such case, the double helix structure can be deformed on surface by interaction between DNA molecules and the surface.

The other is deformation in solution. Cation also stabilizes the double helix structure because cation screens negative charge in phosphate group of DNA. The denaturing temperature of double helix structure (T_m) is fluctuated by concentration of cation ($[M^+]$):

$$\Delta T_m = 16.6 \log[M^+] \qquad (3\times10^{-4} < [M^+] < 0.2M)$$

where ΔT_m is variation of T_m. In this experiment, T_m was decreased by 35 °C because the concentration of DNA solution became 100 times smaller by dilution with water. This suggests that the dilution make the double helix structure unstable in solution.

The deformation mechanism of DNA molecule and interaction between DNA and surface are still unclear. However, it has been found that NC-AFM provides local double helix structure of DNA molecule. This shows a capability of NC-AFM for observation of bio-material including DNA.

4.4 Conclusion

We have successfully applied NC-AFM to observe double-stranded DNA deposited on Cu(111) surface using a shape-controlled tip. The resulting NC-AFM images revealed the double-helix structure that has not been possible to obtain using AFM. The most frequently value of the

observed pitch lengths was consistent with that of Watson-Crick model. However, the pitch lengths were widely distributed in the range of 2-7 nm and the height was 1 nm suggesting the deformation of DNA on the surface. This deformation might be caused by reducing the base stacking energy and/or concentration of cation. These results prove that NC-AFM is useful to reveal DNA's properties.

4.5 References

[1] S. Heike, T. Hashizume and Y. Wada: J. Vac. Sci. & Technol. B **14** (1996) 1522.

[2] T. Kanno, H. Tanaka, T. Nakamura, H. Tabata, T. Kawai: Jpn. J. Appl. Phys. **38** (1999) 606.

[3] H. Tanaka, C. Hamai, T. Kanno, T. Kawai: Surf. Sci. **432** (1999) L611.

[4] C. Hamai, H. Tanaka, T. Kawai: J. Vac. Sci. Technol. B**17** (1999) 1313.

[5] R.D. Deegan, O. Bakajin, T.F. Dupont, G. Huber, S.R. Nagel, T.A. Witten: Nature **389** (1997) 827.

[6] Gissible: Science **267** (1995) 68.

[7] R. Perez, M.C. Payne, I. Stich, K. Terakura: Phys. Rev. Lett. **78** (1997) 678.

[8] I.Yu. Sokolov, G.S. Henderson, F.J. Wicks: Surf. Sci. **381** (1997) L558.

[9] N. Sasaki, M. Tukada: Jpn. J. Appl. Phys. **38** (1999) 192.

[10] B. Anczykowski, D. Kruger, H. Fuches: Phys. Rev. B**53** (1996) 15485.

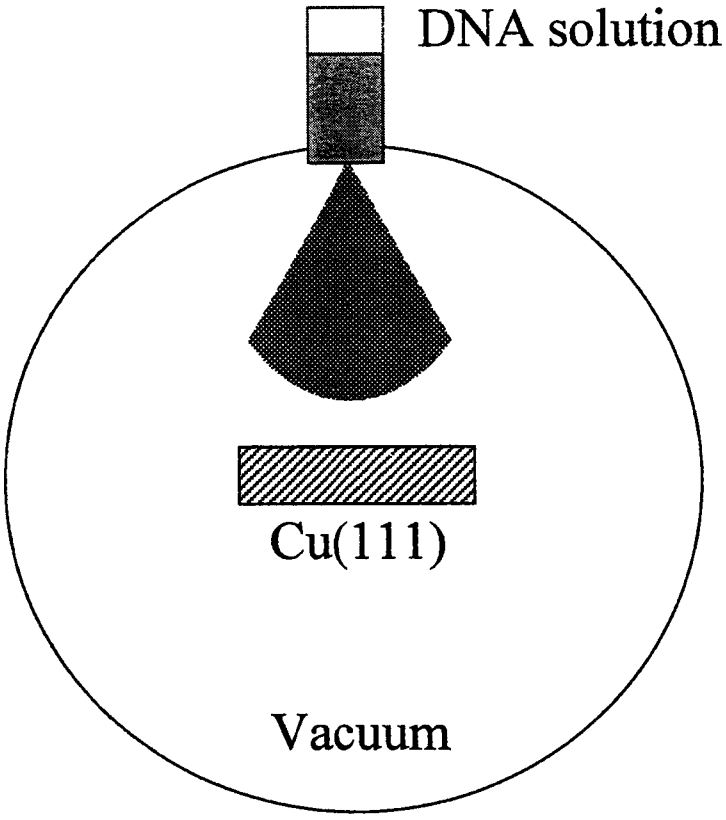

Fig. 4-1
Schematic illustration of pulse injection method.

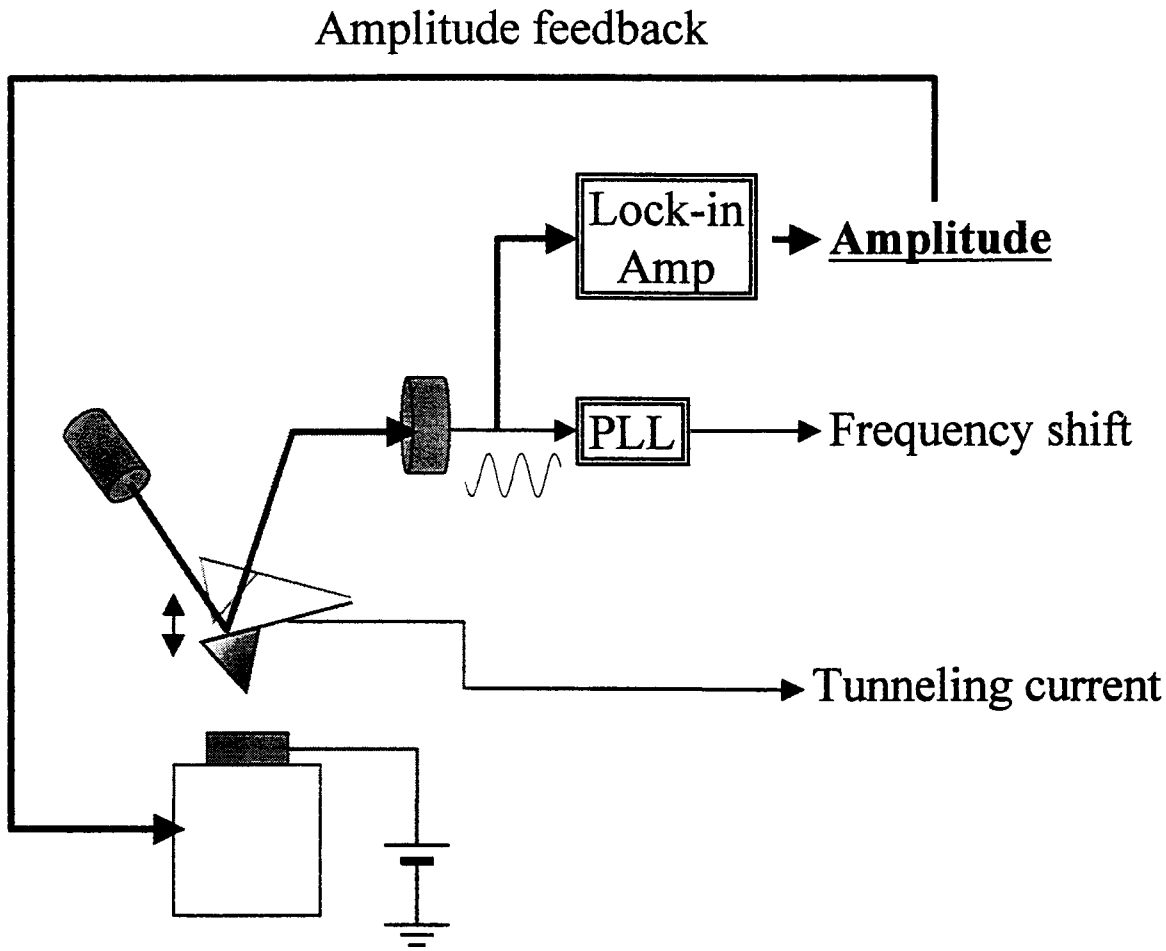

Fig. 4-2
Schematic diagram of NC-AFM.

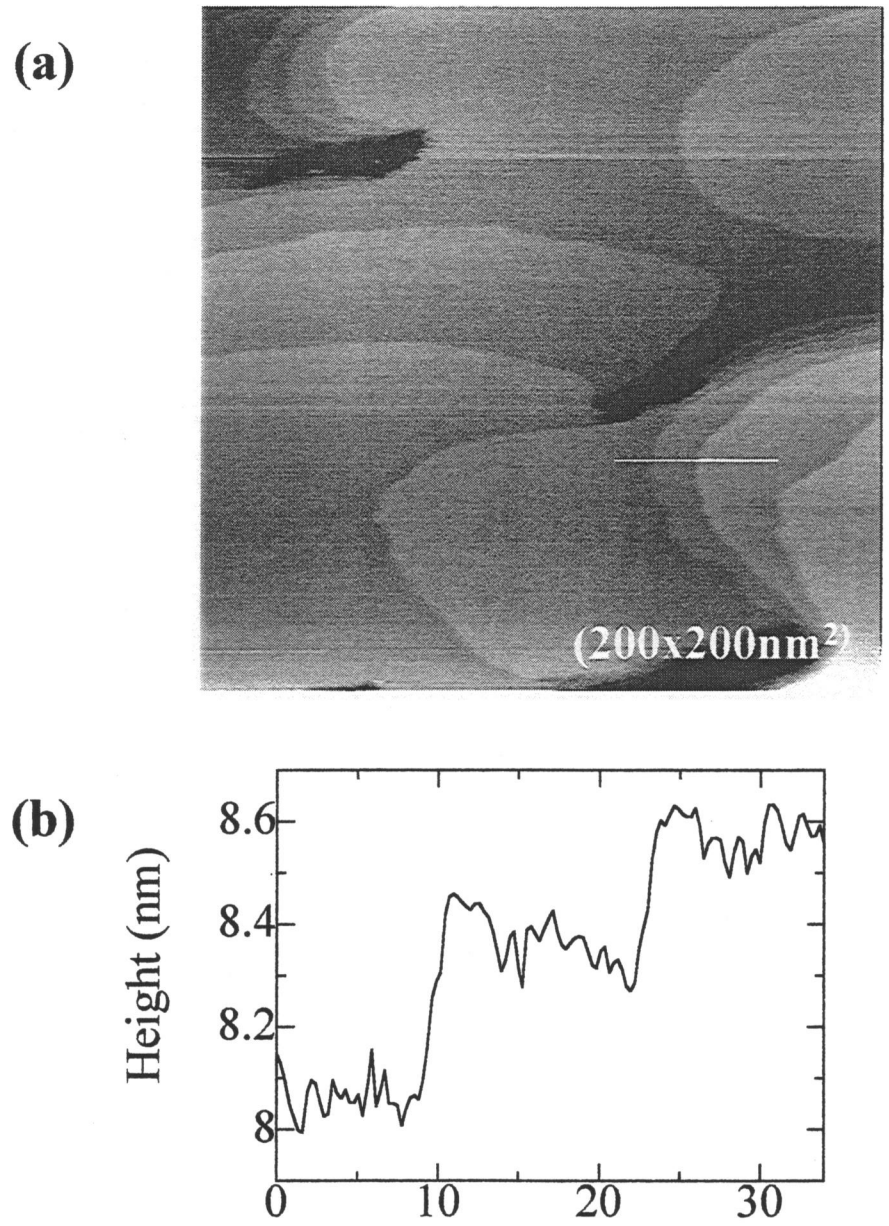

Fig. 4-3
(a) STM image of Cu(111) surface using conductive cantilever. Sample bias and tunneling current were -1 V and 0.1 nA, respectively. (b) Sectional profile of (a) along the line.

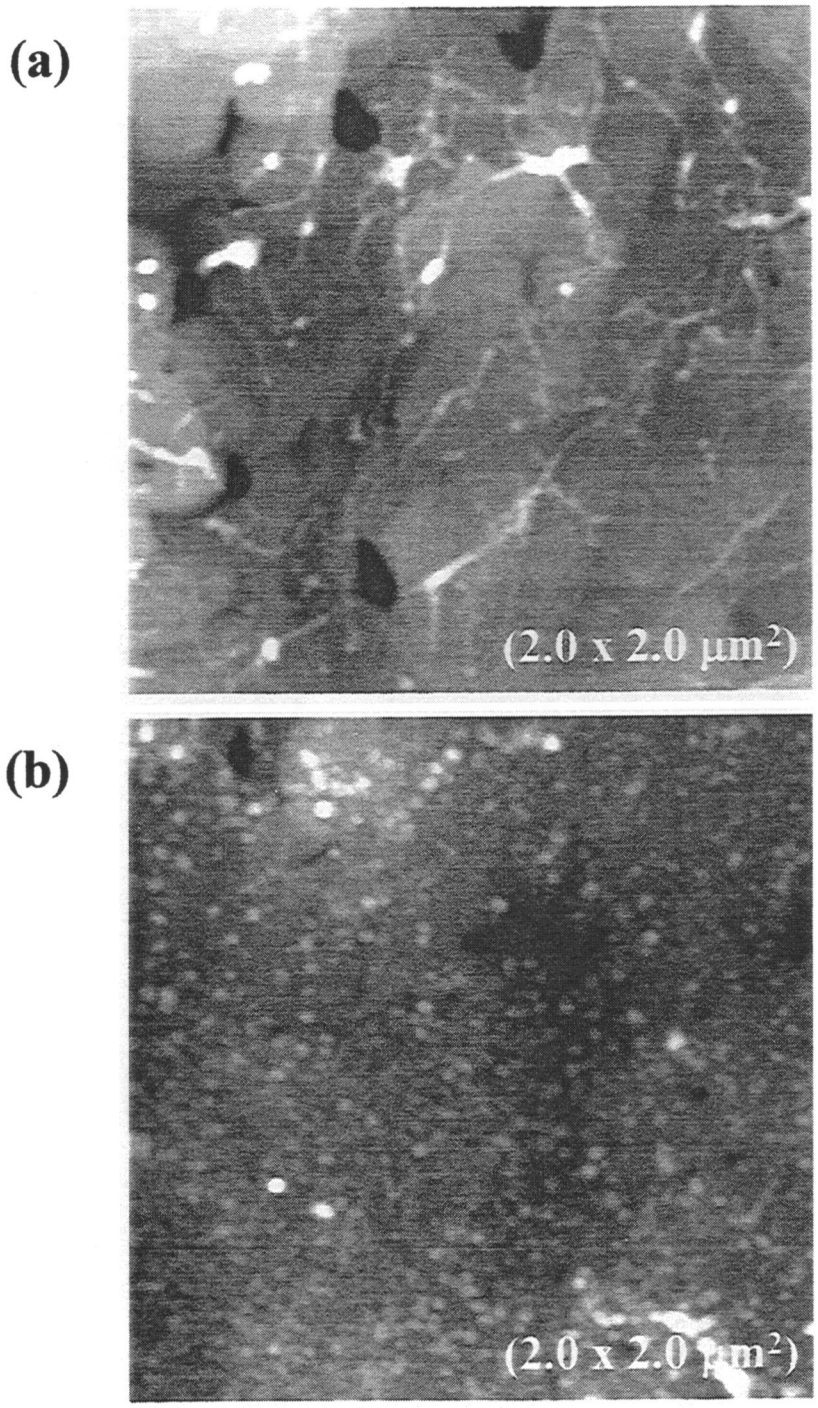

Fig.4-4
TM-AFM images of DNA deposited on Au surface observed (a) at the center and (b) edge of the droplet.

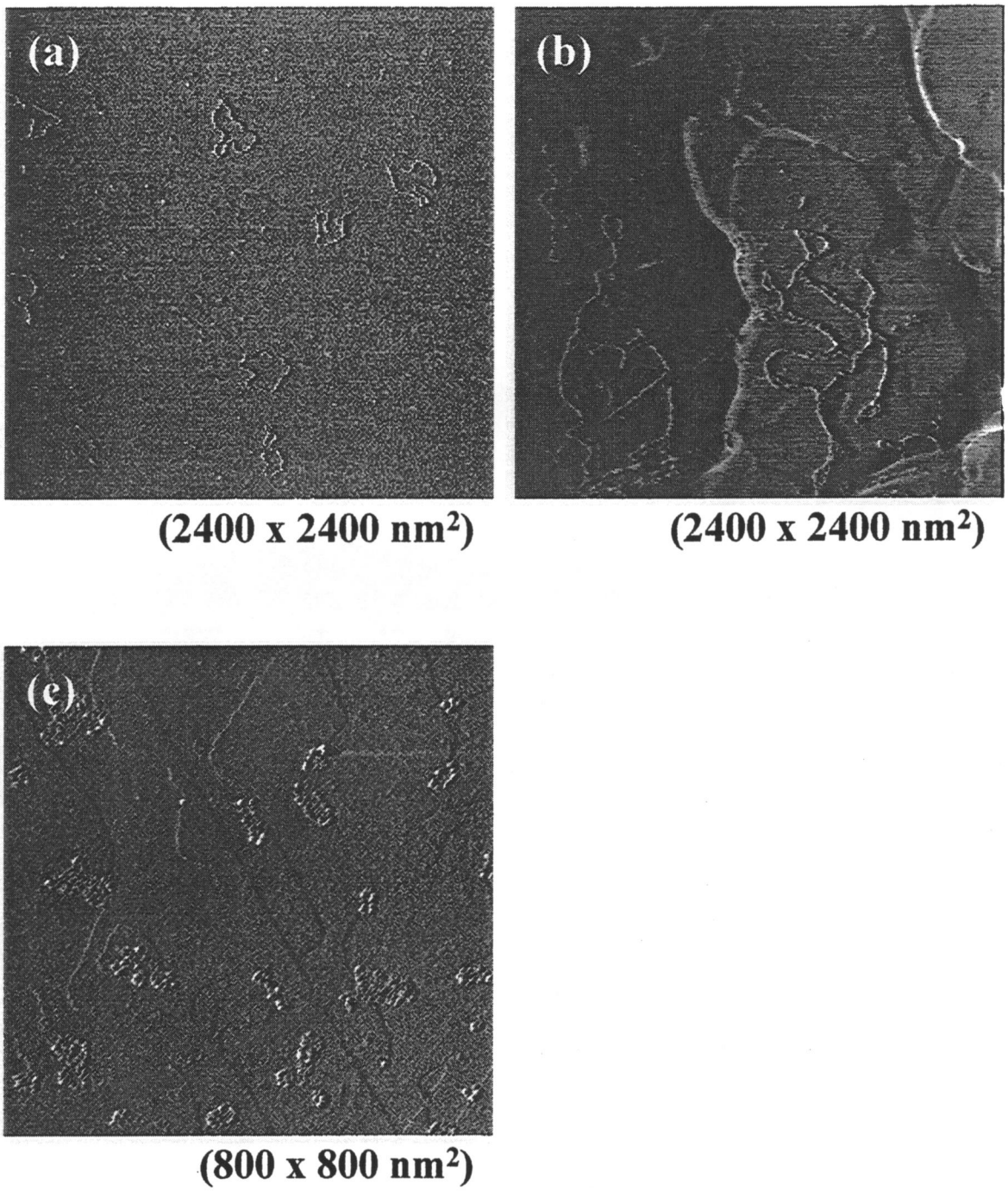

Fig. 4-5
NC-AFM images of Double-stranded DNA deposited (a) on mica and (b) on Au surface by drop-and-dry method and (c) on Au surface by pulse injection method.

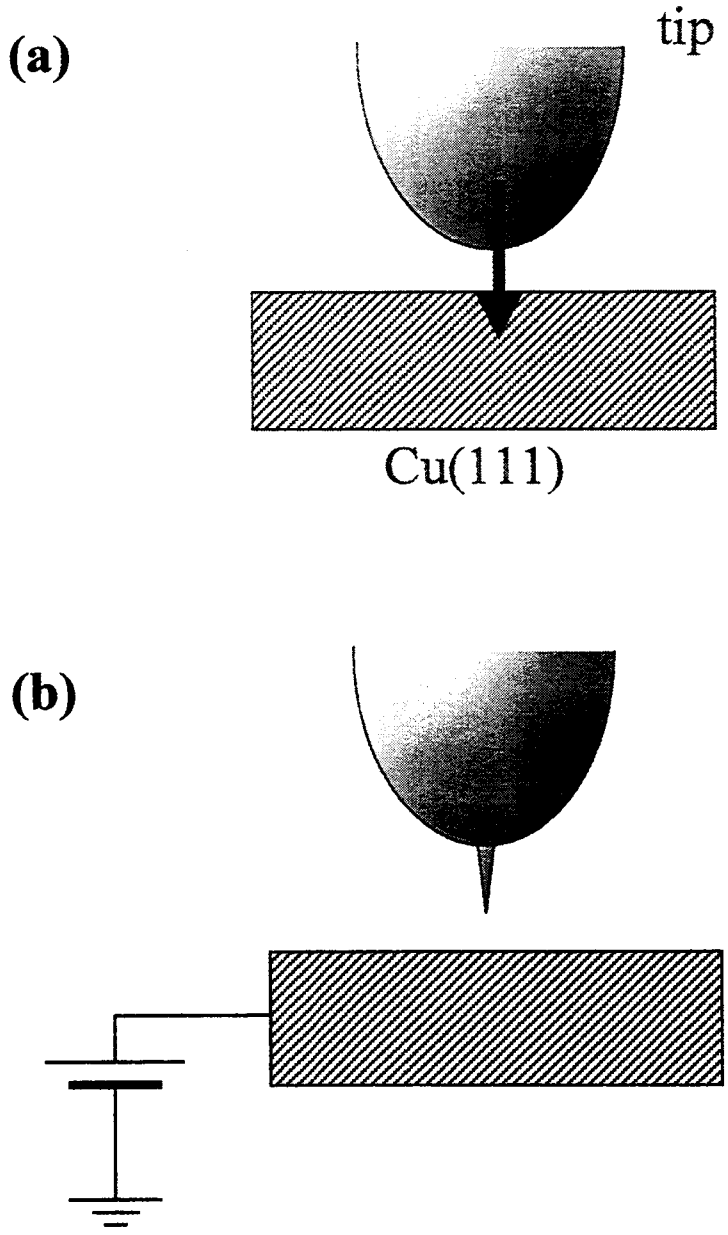

Fig. 4-6
Scheme of tip sharpening process. (a) Tip is pushed to the surface with a load of 0.1-1 μN for removing SiO_2 layer. (b) Bias voltage of +/-10 V is supplied between tip and surface for forming the needle-shaped tip.

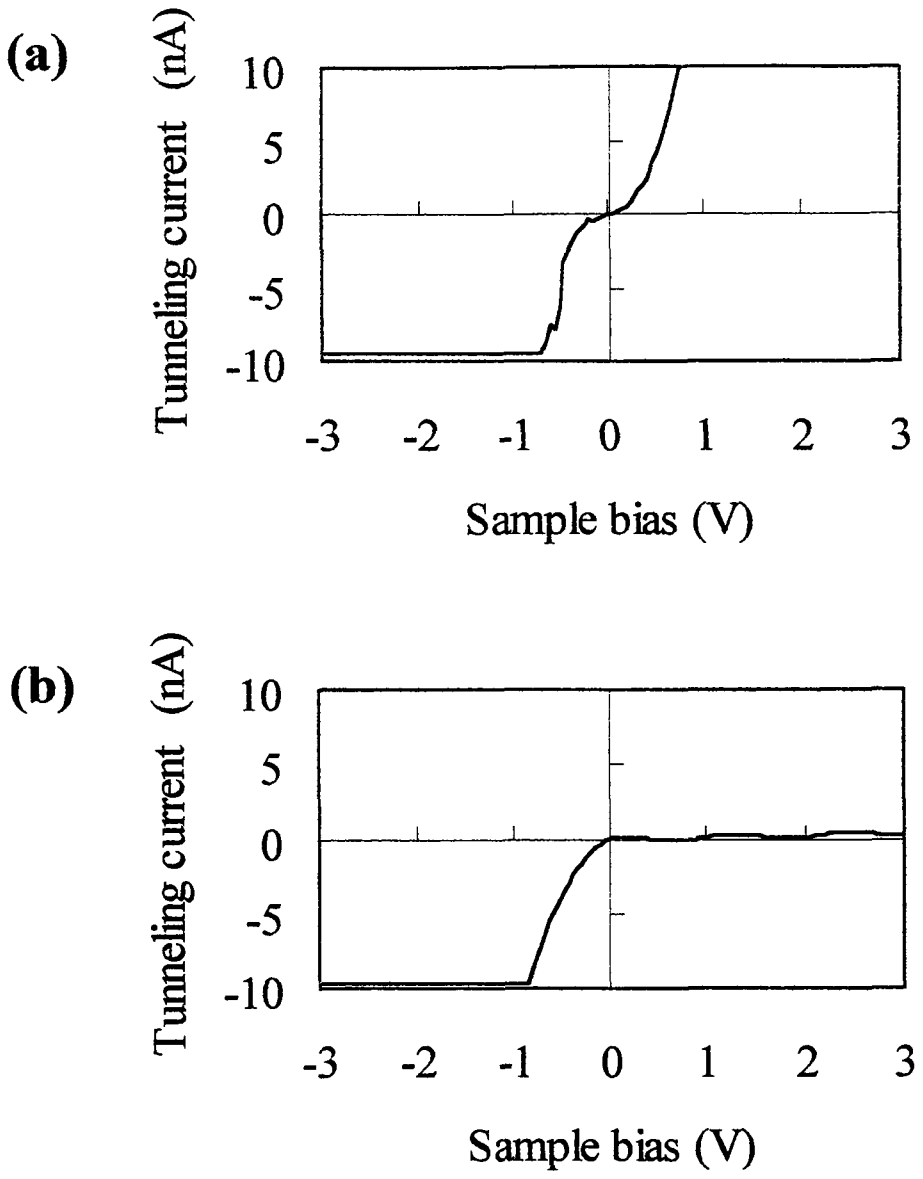

Fig. 4-7
Tunneling current spectra measured on Cu(111) surface using conductive cantilever: (a) before and (b) after supplying high bias voltage of +/-10 V.

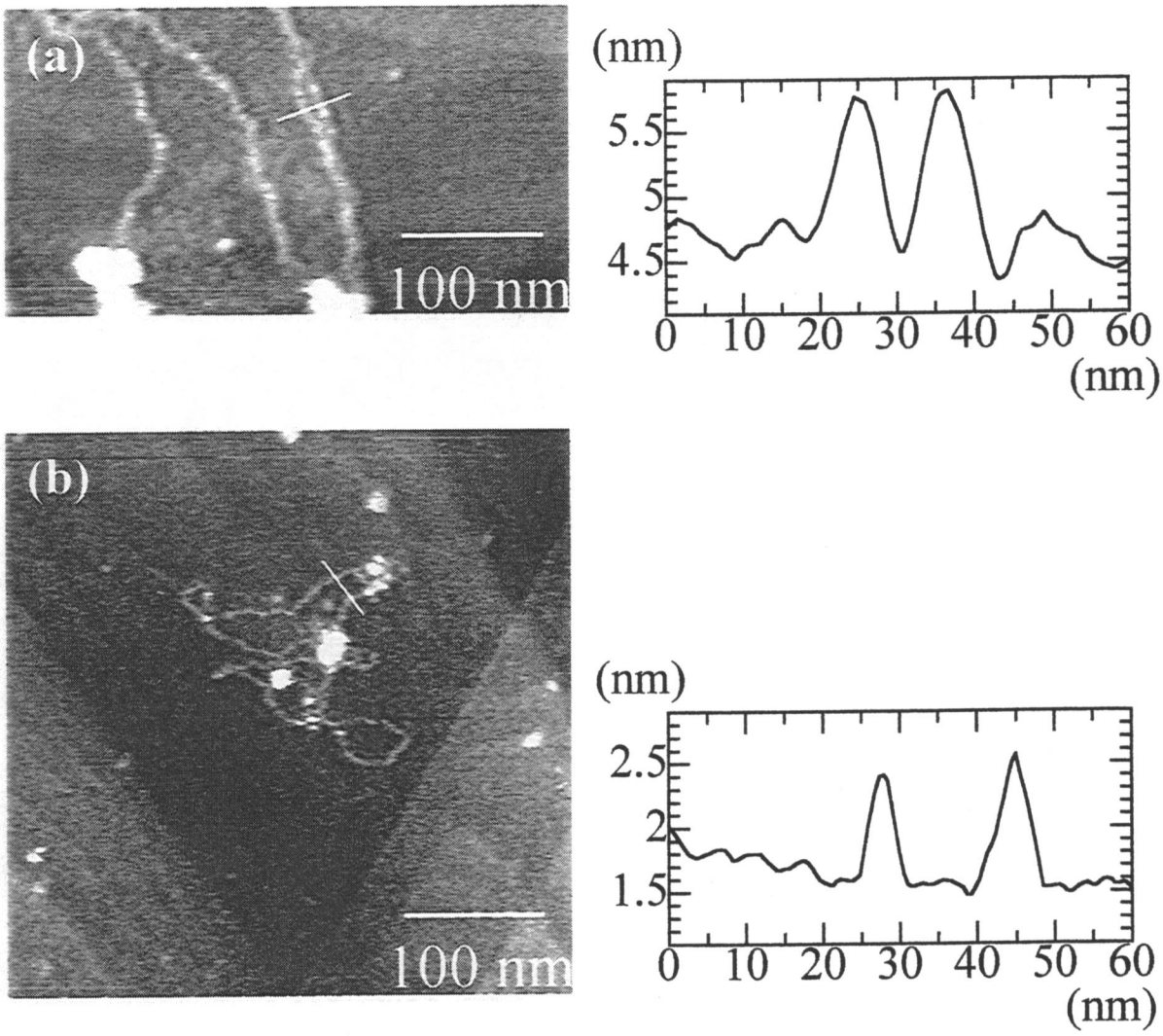

Fig. 4-8
NC-AFM images and sectional profiles along the lines (a) before and (b) after tip sharpening.

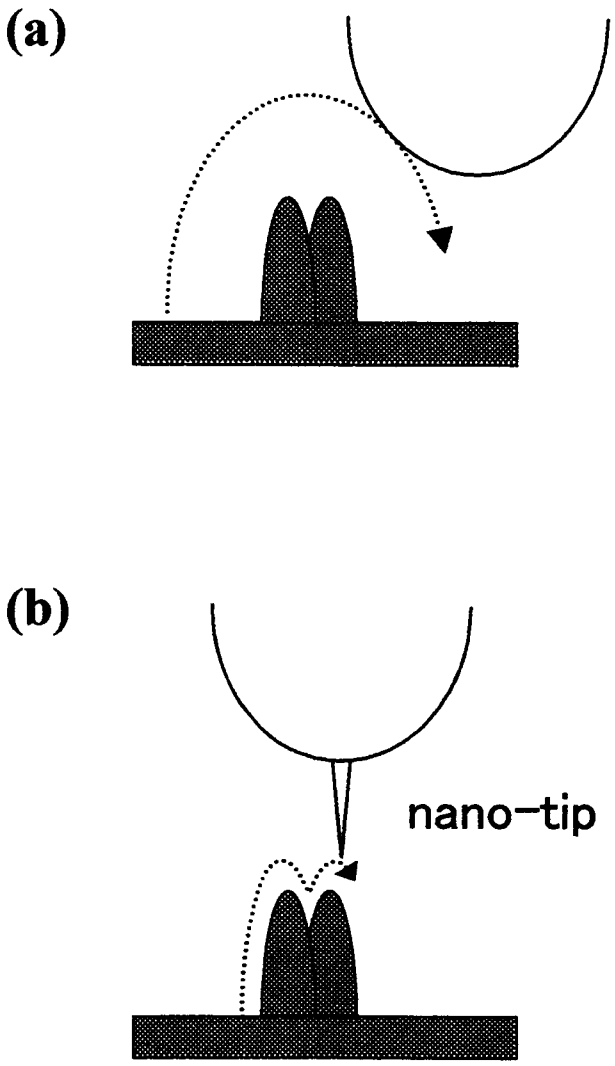

Fig. 4-9
Schematic illustration of imaging mechanism for NC-AFM in case of (a) dull tip and (b) sharp tip.

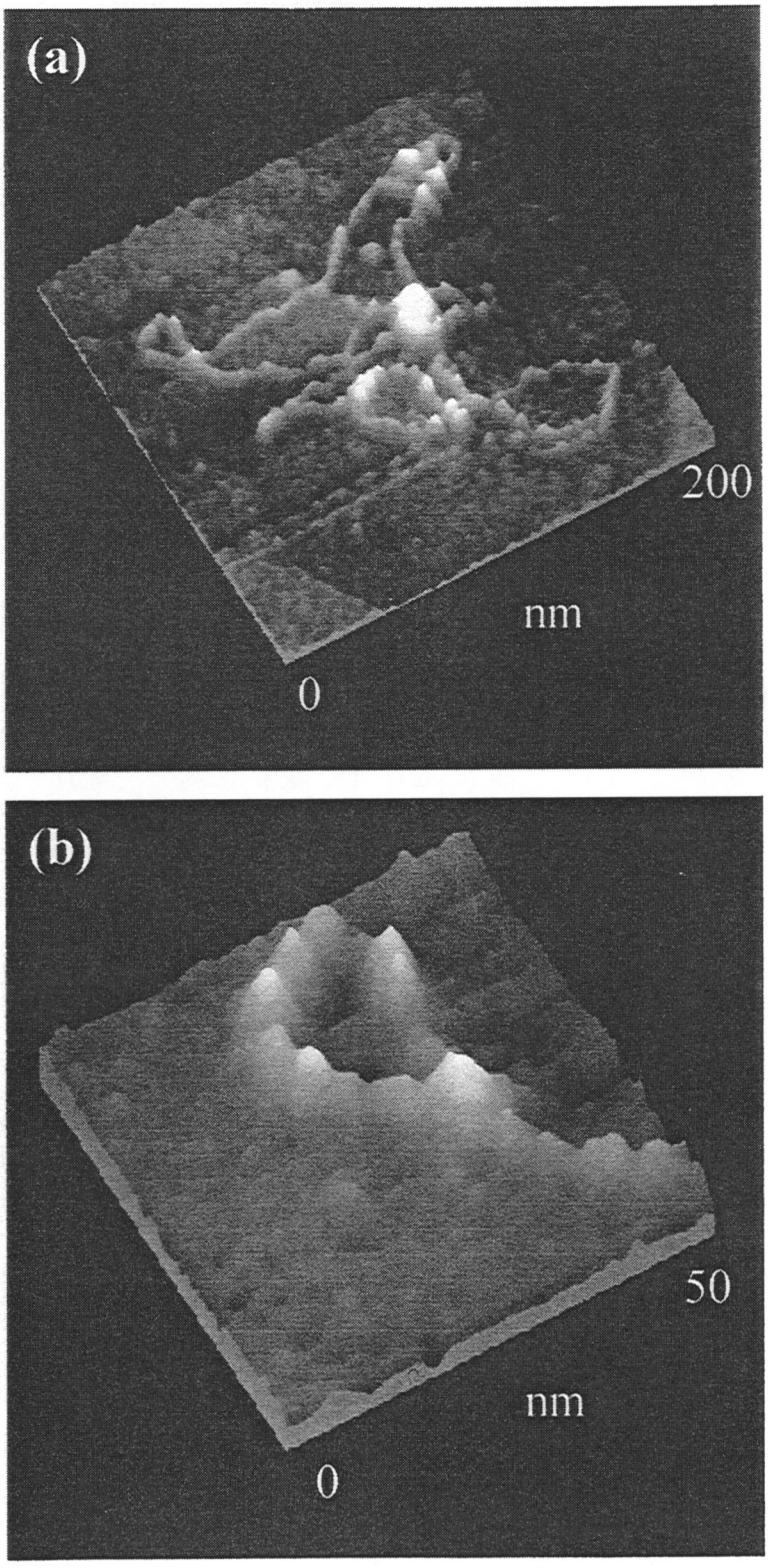

Fig. 4-10
High resolution images of double-stranded DNA observed by NC-AFM. (b) is a magnified image of (a).

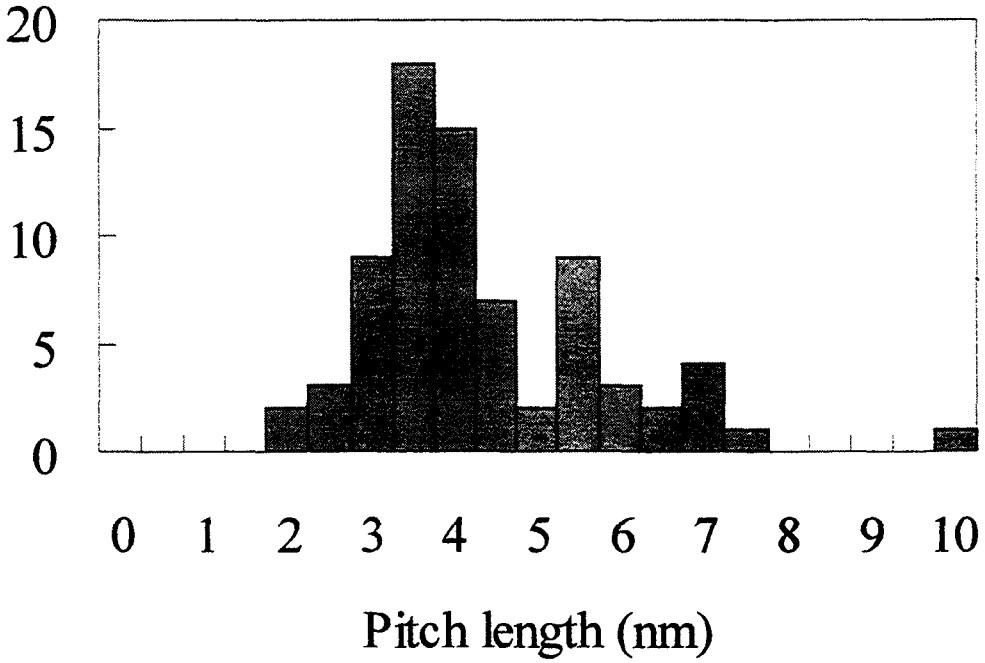

Fig. 4-11
Distribution of the pitch length of double-stranded DNA observed by NC-AFM.

Chapter 5

Multi-mode SPM observation

Chapter 5

Multi-mode SPM observation

5-1 Introduction

One of the most important issues for DNA observation is imaging of local electronic structure of DNA (e.g. density of states: DOS). An isolate nucleic acid base shows the characteristic bias voltage dependence in scanning tunneling microscopy (STM) observation [1,2]. This result shows possibilities to distinguish four kinds of nucleic acid bases and determine base sequence with STM. Recently, DNA based nano-scale devises have been proposed [3-8]. Many research groups have investigated the conductivity of DNA [9-13]. These results suggest that conductivity of DNA is related to energy levels of nucleic acid bases and its sequence. However, it is still unclear.

In this chapter, multi-mode SPM observation of DNA molecule is described. In the multi-mode SPM, frequency shift image, which gives us information related to topography, was simultaneously observed with STM image using conductive cantilevers. The results revealed the relationship between the STM image and the topography of DNA molecule. This is a great advantage of the multi-mode SPM to observe local electronic structure of DNA molecule.

5-2 Experimental

Fig. 5-1 shows a schematic diagram of the multi-mode SPM. Tip-sample distance was controlled by tunneling current with a conductive cantilever which was oscillated at its resonance frequency (~300 kHz) by applying positive feedback. The tunneling current was averaged through

STM pre-amplifier whose time constant is ~1 ms. Frequency shift was observed by optical reflection method though phase-locked-loop (PLL) circuit. The STM image and the frequency shift image were simultaneously obtained in a scan using this operation mode. The sample bias voltage and the average tunneling current were set to +3 V and 10 pA, respectively.

The cantilever and sample preparation are described in chapter 4

5-3 Results and discussion

Fig. 5-2 shows (a) a STM image and (b) a simultaneously observed frequency shift image obtained by multi-mode SPM. In the STM image (Fig. 5-2(a)), a multi atomic step of Cu(111) having a height of 0.8 nm (at the center) and a single atomic step having a height of 0.2 nm (at the upper-left side) can be seen. At the center of this image, double-stranded DNA, having many protrusions whose periodicity is 3-5 nm, can also be seen. The period of the protrusions is consistent with the Watson-Crick model, indicating that the double helix structure can be observed by the multi-mode SPM.

The average frequency shift in multi-mode SPM at the bias voltage of 3.0 V was 100-200 Hz. The typical frequency shift in NC-AFM observation (frequency shift feedback) without bias voltage was 5-30 Hz. This indicates that frequency shift in multi-mode SPM (100-200 Hz) mainly arises from electrostatic force caused by bias voltage. In spite of the presence of electrostatic force, the DNA molecule was also observed in frequency shift image as shown in Fig. 5-2(b) because the electrostatic force forms a uniform background over the surface. The frequency shift image of DNA molecule is quite similar to the STM image. On the other hand, the Cu(111) steps in the frequency shift image show low contrast, and many particles can be seen only in the frequency shift image.

Figure 5-3 shows sectional profiles of (a) STM image and (b) frequency shift image across the DNA molecule. The corrugations of DNA molecule in the STM image (STM height) and in frequency shift image (Δf corrugation) are 0.8 nm and 4.5 Hz, respectively. On the other hand, at the Cu(111) step (indicated by arrows in Fig. 5-4(b)) which have 0.2 nm height in the STM image (Fig. 5-4(a)), Δf corrugation are 0 Hz as shown in Fig. 5-4(b). The Cu(111) steps in the frequency shift image are observed by transient response of feedback loop. In contrast, the frequency shift image (Fig. 5-5(b)) shows many particles which might be EDTA (Ethylene-diamine-tetraacetic acid) molecules included in buffer solution. The Δf corrugation of the molecule is 3.5 Hz. This molecule can not be seen in the STM image as shown in Fig. 5-5(a).

The correlation between STM height and Δf corrugation in multi-mode SPM is plotted in Fig. 5-6. Solid circle, open square and cross show DNA molecules, Cu(111) steps and EDTA molecules, respectively. Δf corrugation of DNA molecules is roughly proportional to the STM height. On the other hand, the data for Cu(111) steps are located on the horizontal axis and the data for EDTA molecules are distributed near the vertical axis. These results can be explained as follows. The Δf corrugation is caused by a change of tip-sample distance. The tip-sample distance is kept constant above and below the Cu(111) steps with constant tunneling current. Therefore, the Δf is not changed at the Cu(111) steps. In contrast, in the case of EDTA molecule, the tip-sample distance become close on the molecules because EDTA molecules can not be observed in STM images. This originates the Δf corrugation on the molecules. These results suggest that the tip-sample distance become close on DNA molecule in multi-mode SPM.

Fig. 5-7 shows the height of DNA molecules observed by multi-mode SPM (i.e., STM height) and by NC-AFM (NC-AFM height). NC-AFM operation is described in chapter 4. The STM heights are distributed in the range of 0.1-0.8 nm and the average value is 0.52 nm. The NC-AFM heights are distributed in the range of 0.4-0.8 nm and the average value is 0.69 nm. This indicates that STM height is 0.17 nm smaller than the height of DNA molecule. This is consistent with the results of the multi-mode SPM observation.

Fig. 5-8 shows the schematic illustration of relationship between STM image in multi-mode SPM and topography of DNA molecule. A tip traces a contour of DNA molecule with constant tunneling current but the STM height in multi-mode SPM is 2 Å smaller than the height of DNA molecule.

Tunneling current (I_t) is described as $I_t \propto \rho \exp(-\sqrt{\Phi_e} z)$, where ρ, Φ_e and z are local density of states (LDOS), effective tunneling barrier height and tip-sample distance, respectively. In Multi-mode SPM observation, the tip-sample distance on DNA molecules is closer than that on Cu(111) surface as mentioned above. There are two possibilities of changing the tip-sample distance (z). One is reduction of effective tunneling barrier height (Φ_e) as shown in Fig. 5-9(b). Assuming the tip-sample distance of 7 Å on Cu surface and DNA height of 7 Å, the effective barrier height must decrease by 2.4 eV on DNA. Compared with the value for another organic molecule (e.g. 1 eV for an adenine molecule on $SrTiO_3$ [14]), this value is quite large.

The most provable mechanism is electron tunneling from a DNA molecule as shown in Fig 5-9(a). In this case, DNA molecule must have DOS, which might hybridizes with the Cu(111) surface, at 3 eV above the Fermi level. The experimental results show that the tip-sample distance on

DNA molecule is 2 Å smaller than that on Cu(111) surface, suggesting that DOS of DNA is two order smaller than that of Cu(111) surface. Furthermore, the Δf corrugation in DNA molecules reveals variation of LDOS in a molecule because uniform effective barrier height over the molecule can be assumed (Φ_e=constant). These results show the capability of multi-mode SPM to analyze LDOS of DNA molecule.

5-4 Conclusion

The multi-mode SPM observation of DNA molecule has been performed on Cu(111) surface. The double helix structure was observed by the multi-mode SPM. The results indicate that DOS of DNA molecule is two order smaller than that of Cu(111) surface, and LDOS in DNA molecule can be observed as a function of Δf by multi-mode SPM.

Further improvement is necessary to estimate LDOS of DNA molecule quantitatively. However, multi-mode SPM allows us to define the local electric structure of DNA molecule on the surface.

5-5 References

[1] H. Tanaka, T. Kawai: J. Vac. Sci. Technol. B**13** (1995) 1411.

[2] M. Kasaya, H. Tabata, T. Kawai: Surf. Sci. **406** (1998) 302.

[3] A.P Alivisatos, K.P Johnsson, X. Peng, T.E. Wilson, C.J. Loweth, M.P. Bruchez Jr., P.G. Schultz: Nature **382** (1996) 609.

[4] C.A. Mirkin, R.L. Letsinger, R.C. Mucic, J.J. Storhoff: Nature **382** (1996) 607.

[5] E. Braun, Y. Eichen, U. Sivan, G. Ben-Yoseph: Nature **391** (1998) 775.

[6] E. Winfree, F. Liu, L. Wenzler, N.C. Seeman: Nature **394** (1998) 539.

[7] C. Mao, W. Sun, N.C. Seeman: J. Am Chem. Soc. **121** (1999) 5443.

[8] C.M. Niemeyer: Appl. Phys. A**68** (1999) 119.

[9] M.D. Purugganan, C.V. Kumar, N.J. Turro, J.K. Barton: Science **241** (1988) 1645.

[10] C.J. Murphy, M.R. Arkin, Y. Jenkins, N.D. Ghatlia, S.H. Bossmann, N.J. Turro, J.K. Barton: Science **262** (1993) 1025

[11] S. Priyadarshy, S.M. Risser, D.N. Beratan: J. Phys. Chem. **100** (1996) 17678.

[12] S.O. Kelley, J.K. Barton: Science **283** (1999) 375.

[13] H.W. Fink, C. Shonenberger: Nature **398** (1999) 407

[14] R. Akiyama, T. Matsumoto, T. Kawai: J. Phys. Chem. B103 (1999) 6103

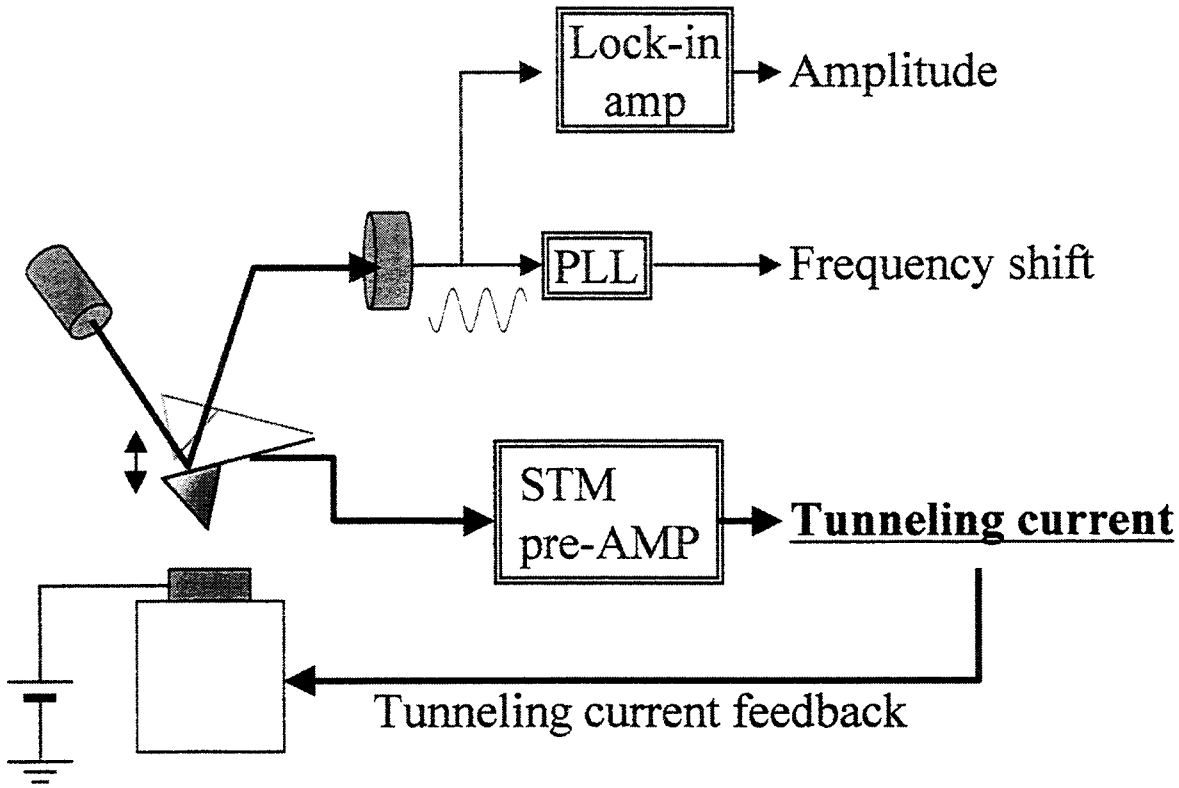

Fig. 5-1
Schematic diagram of multi-mode SPM.

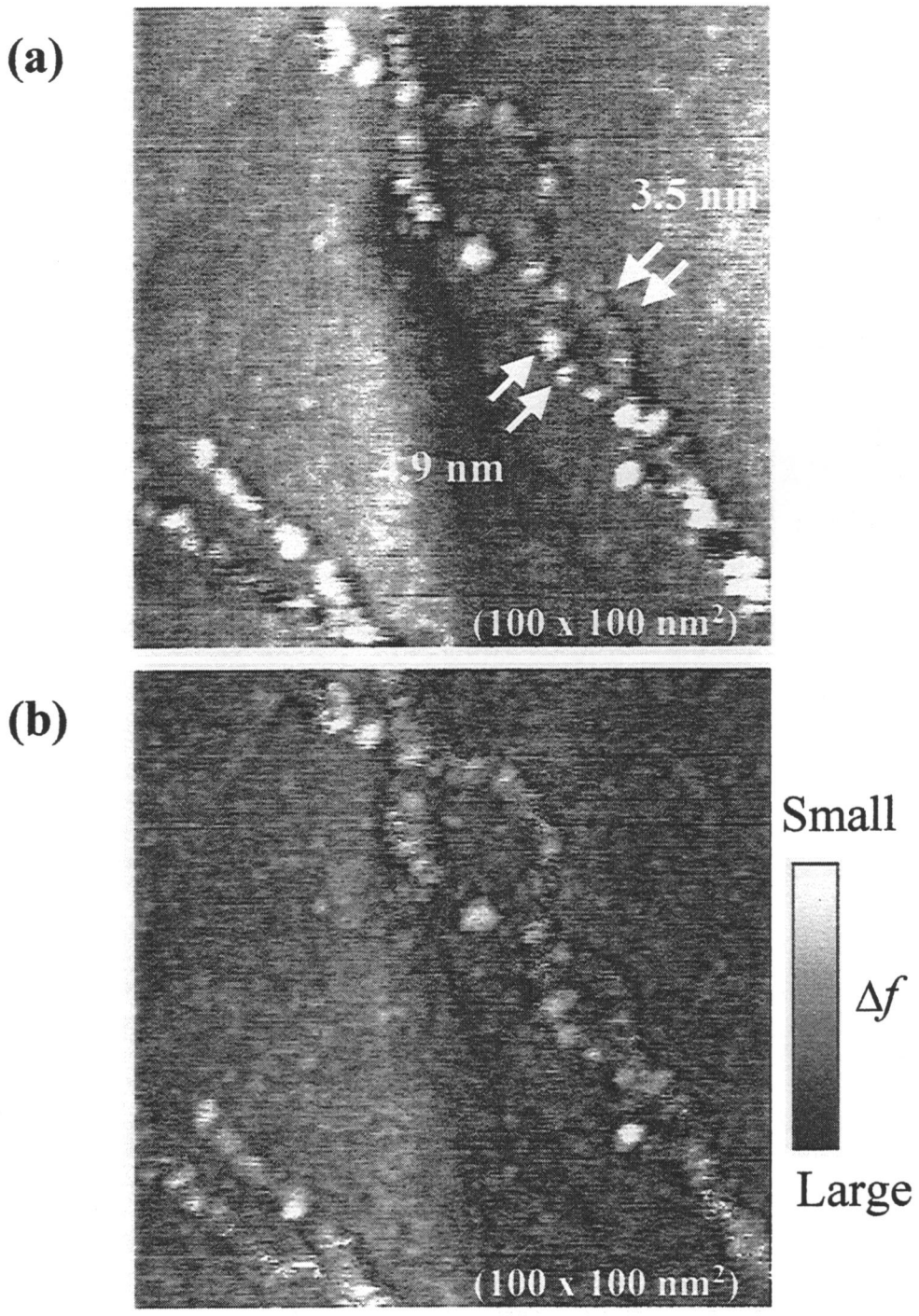

Fig.5-2
Double-stranded DNA images obtained by multi-mode SPM.
(a) STM image at sample bias of 3V and tunneling current of 10pA.
(b) Frequency shift image simultaneously observed with (a)

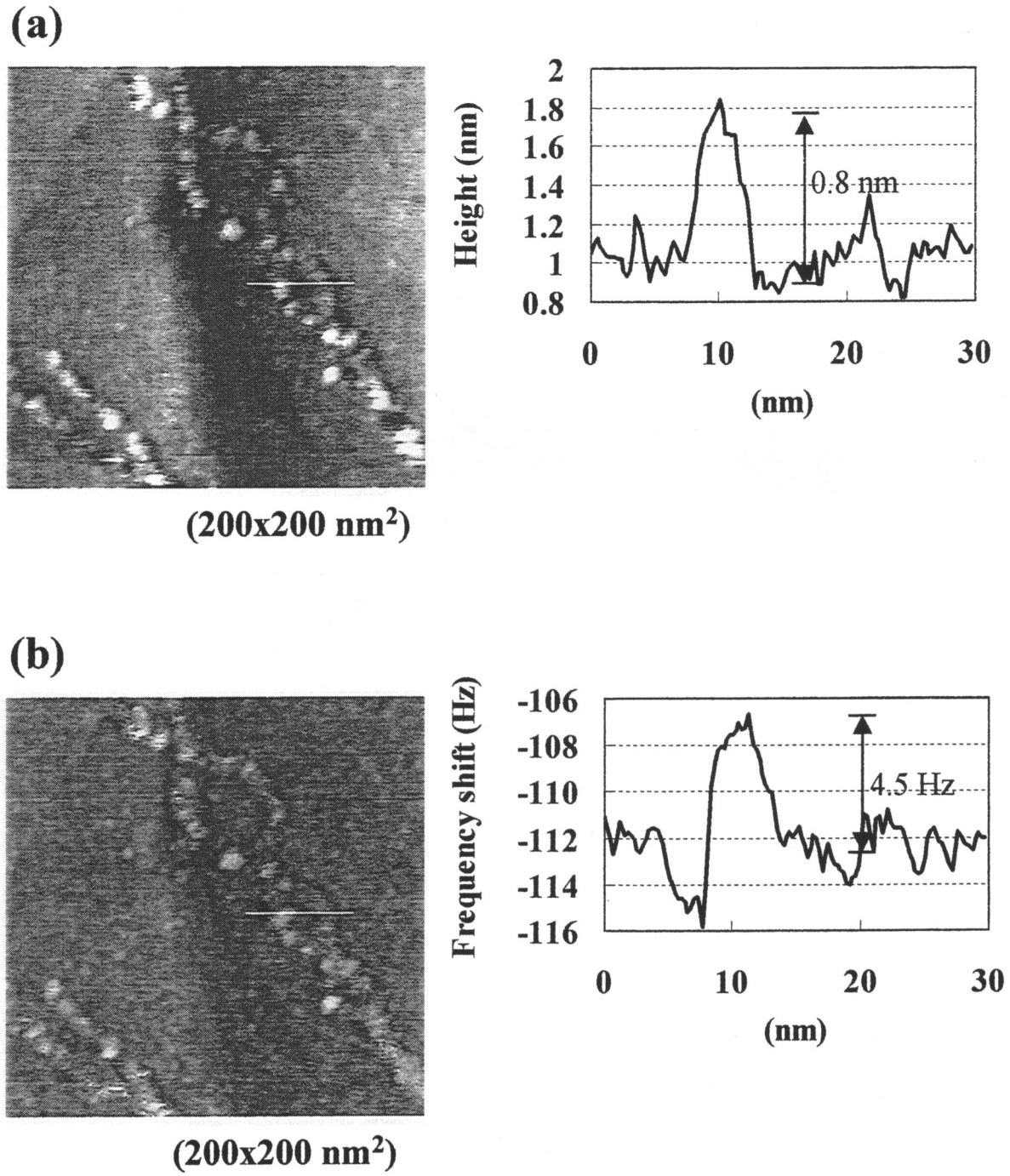

Fig. 5-3
Sectional profiles across the DNA molecule in (a) STM image and (b) frequency shift image.

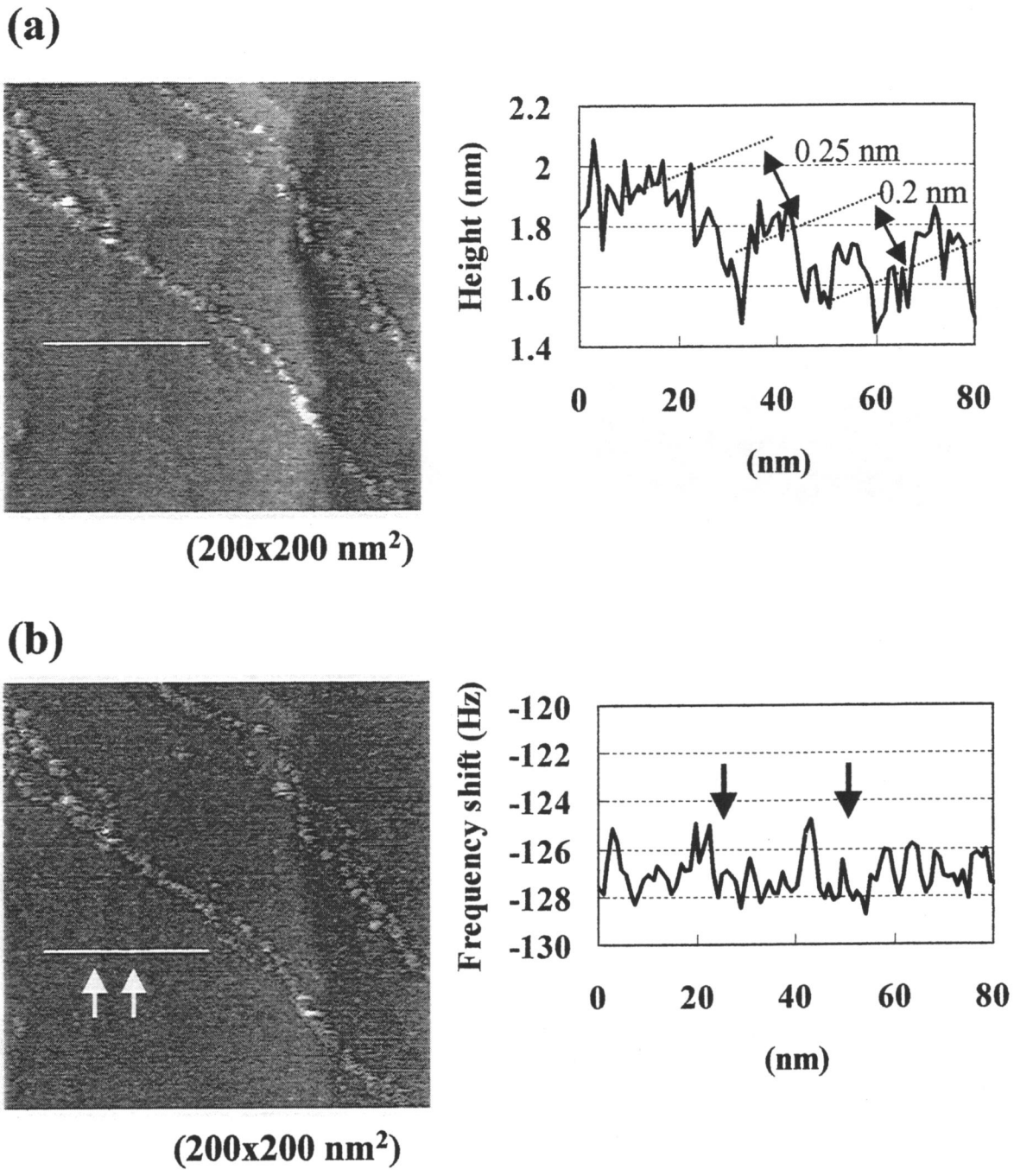

Fig. 5-4
Sectional profiles across the Cu(111) steps in (a) STM image and (b) frequency shift image.

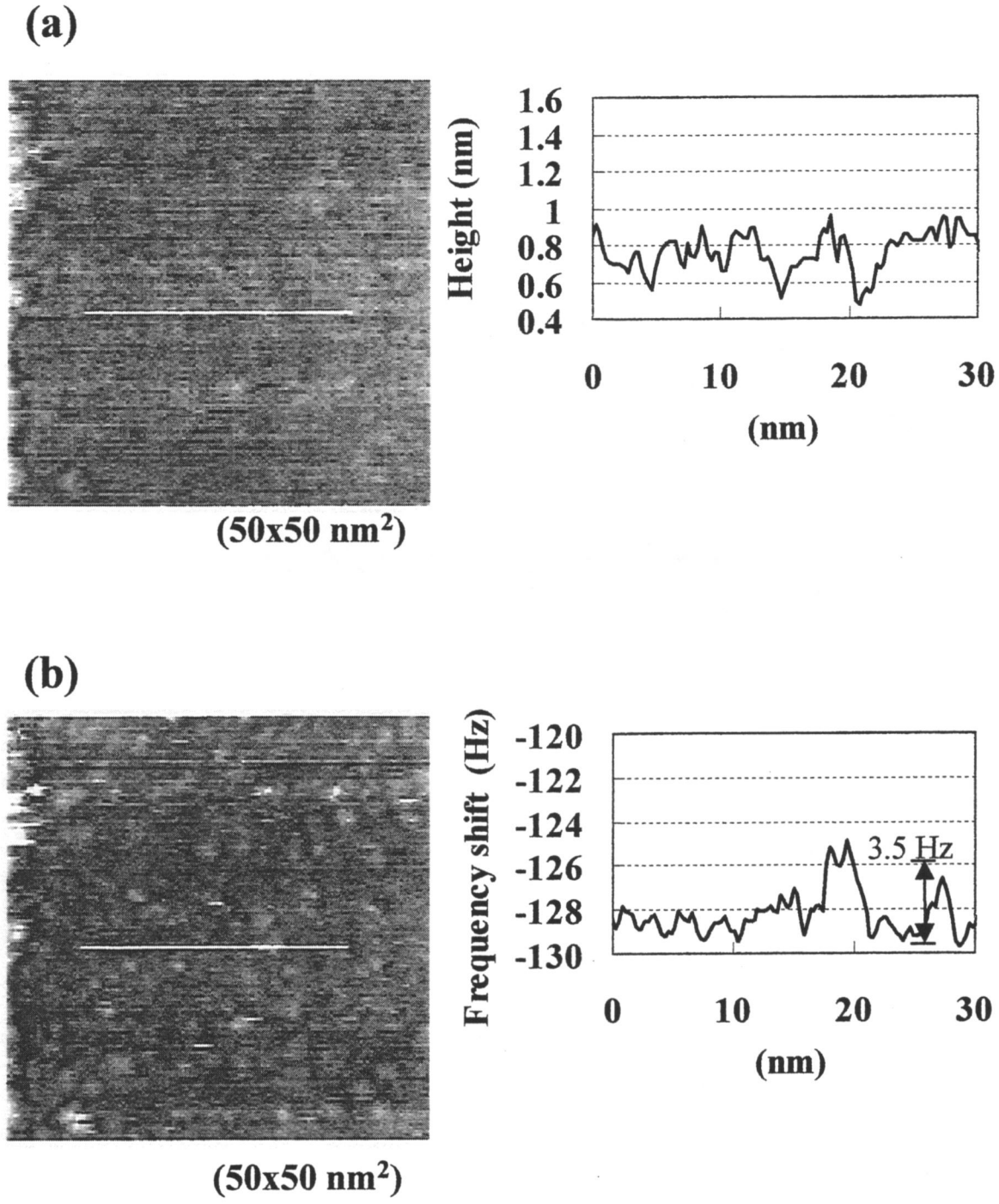

Fig. 5-5
Sectional profiles across the buffer molecule in (a) STM image and (b) frequency shift image.

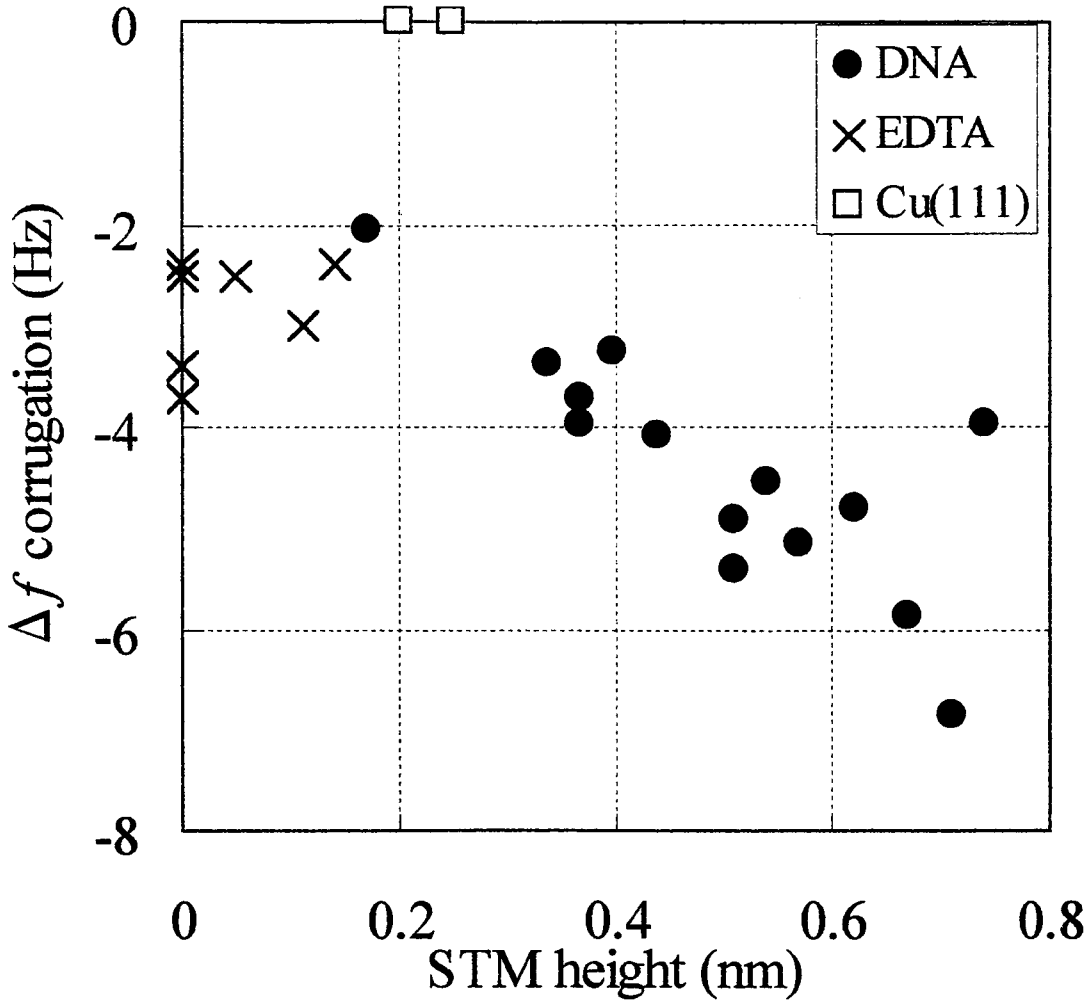

Fig. 5-6
Correlation between corrugation of STM image (STM height) and that of frequency shift image (Δf corrugation). These data were obtained by multi-mode SPM.

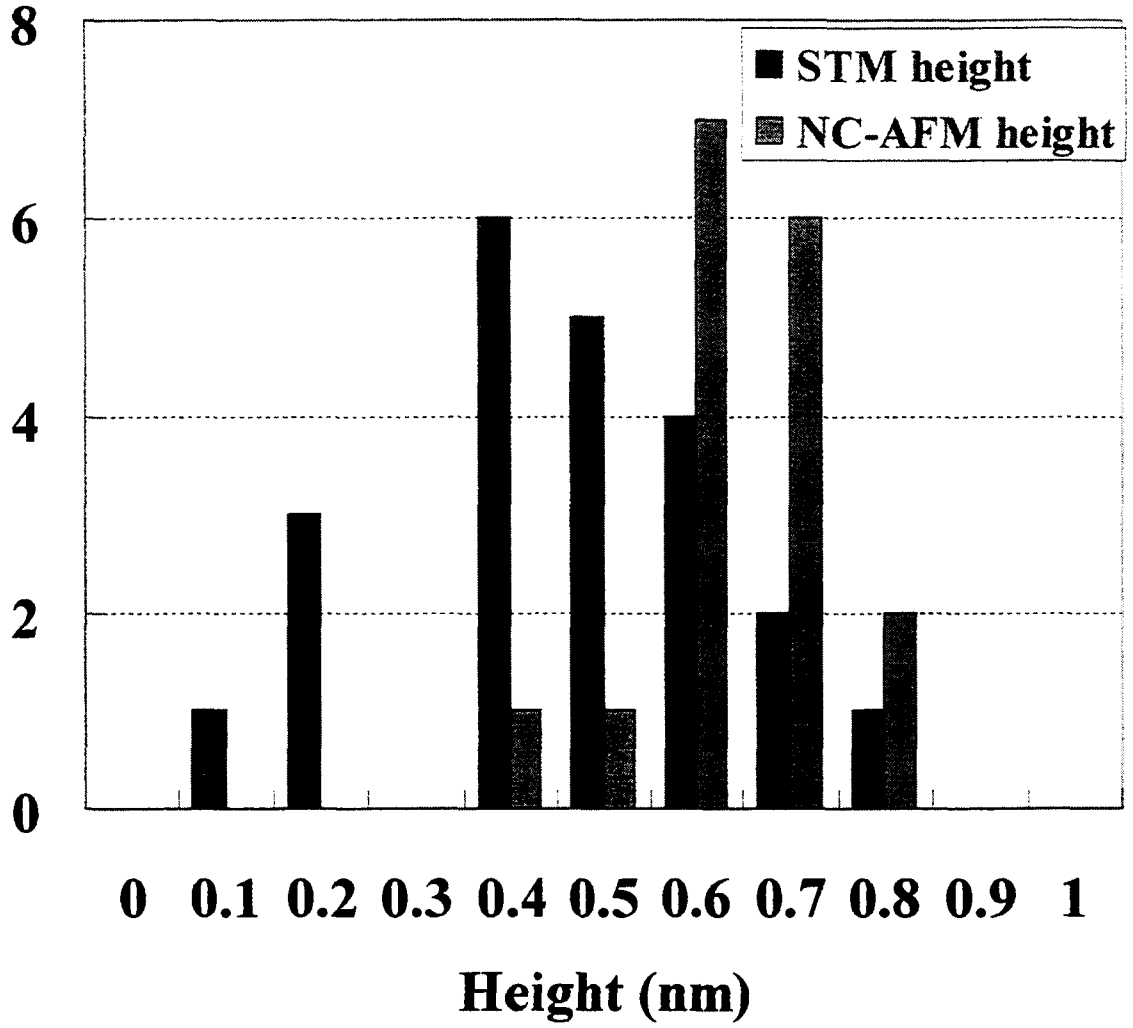

Fig. 5-7
Histogram of heights of DNA molecules observed in STM image in multi-mode SPM (STM height) and NC-AFM image (NC-AFM height).

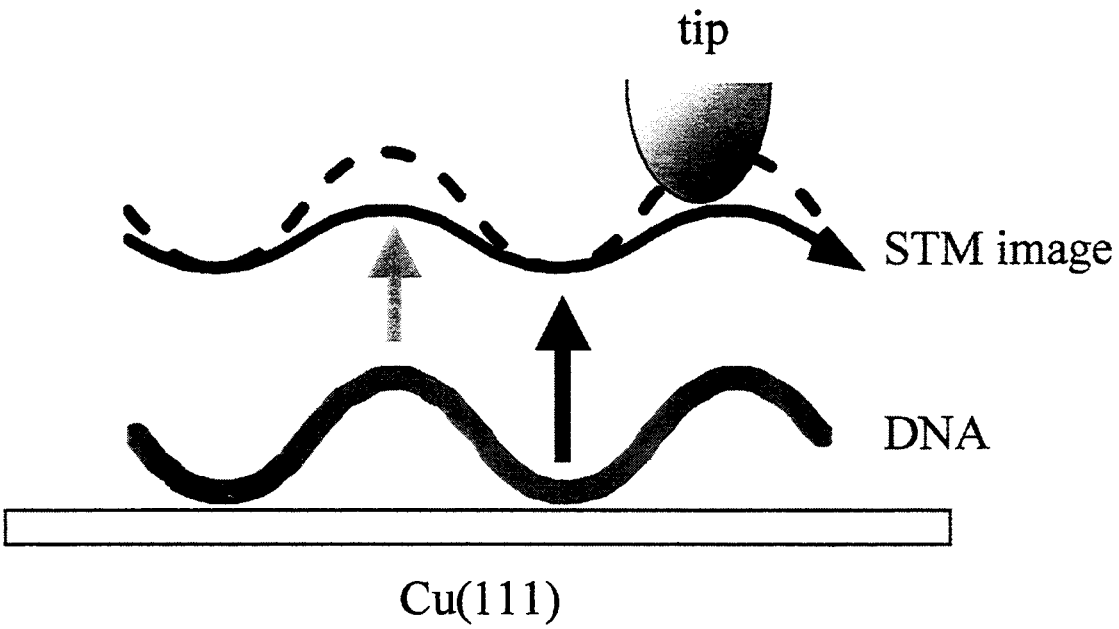

Fig. 5-8
Schematic illustration of the correlation between STM image in multi-mode SPM and topography of DNA molecule. The color of arrows shows the gray scale of frequency shift image in multi-mode SPM.

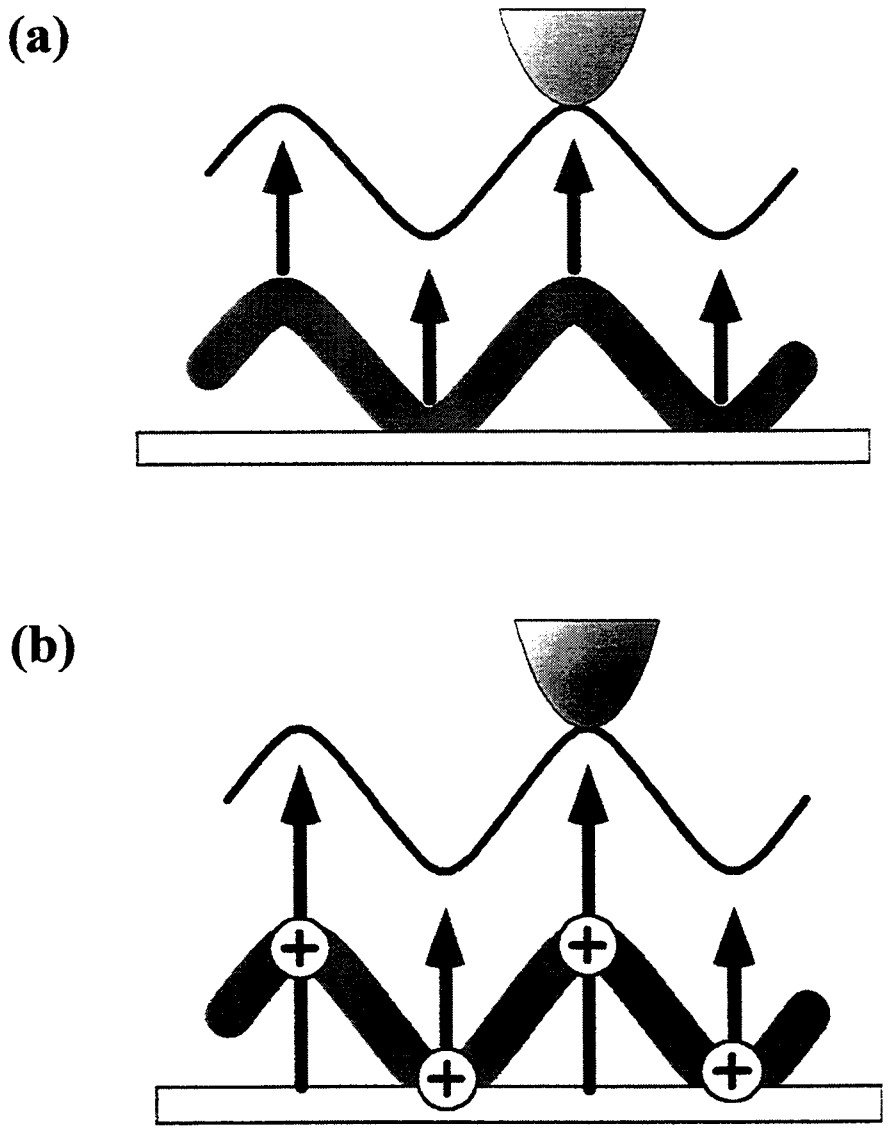

Fig. 5-9
Possible tunneling mechanism of STM observation of DNA molecules. (a) Electrons tunnel form the DNA molecule. (b) Electron tunneling is enhanced by the polarization of DNA molecule.

Chapter 6

General Conclusion

Chapter 6

General Conclusion

NC-AFM and multi-mode SPM observation of DNA molecules have been performed. The periodicity of double helix structure of DNA was successfully observed by improving the sample and tip preparation.

The NC-AFM observation on mica and Cu(111) surface have revealed that it is possible to observe DNA under presence of strong adhesion forces and the most essential factor for high resolution imaging is a shape of a tip. The tip shape is controllable by supplying high bias voltage between tip and sample. The improvement of the tip shape has showed a dramatically change in resolution of DNA images and allowed us to observe the double helix structure using NC-AFM.

Multi-mode SPM observation has revealed the correlation between the STM image and topography of DNA on Cu(111) surface. The density of states of DNA molecule has been estimated as two order smaller than Cu(111) surface. Further improvements are necessary for quantitative measurement. However, the results indicate the capability of multi-mode SPM to make clear the electronic properties of DNA.

Appendix

Controlled conjugation of nanoparticles with single stranded DNA

Appendix

Controlled conjugation of nanoparticles with single stranded DNA

A-1 Introduction

DNA, which carries genetic information, is potentially useful for nano-scale devices. DNA's specific hybridization may allow molecules or clusters to be arranged on nanometer-scale exceeding limitations of photolithography, the patterning size of which is limited up to the wavelength of light (i.e., several hundred nanometers).

Several research groups have formed nano-structures using DNA-based methods [1-3]. Mirkin et al. have controlled an assembly of Au nano-particles in an aggregate structure [2]. Alivisatos el al. have proposed a novel method of organizing Au nano-particles based on Watson-Crick base-pairing interaction [3]. The nano-particles were arranged by pairing an oligonucleotide-Au complex with a DNA template. In these studies, the Au nano-particles are combined with the oligonucleotide by thiol groups.

Conversely, a biotin-streptavidin reaction has been generally used for marking a specific DNA sequence with various particles and phosphorous on biochemical genetics [4,5]. This reaction is able to available for the various applications including optical memory using phosphorous other than the Au nano-particles.

This chapter describes a proposition of a new strategy for the controlled arrangement of nano-particles on long single-stranded DNA (ssDNA) using the hybridization technique and the biotin-streptavidin reaction. This chapter also describes results of observing the controlled one-to-one binding

of Au nano-particles to ssDNA molecules by atomic force microscopy (AFM).

A-2 Experimental

The strategy for the controlled addition of an Au nano-particle to a ssDNA molecule is shown in Fig. A-1. The sequence of the biotinylated oligonucleotide (probe ssDNA) can be chosen to ensure the complete hybridization with the ssDNA template. The probe ssDNA catches only one streptavidin coated Au particle using the biotin-streptavidin reaction, which allows the Au particles to be arranged on the DNA molecule.

The ssDNA template used was M13mp18 (7246 bases, from Takara Shuzo Co., Ltd.). Biotinylated oligonucleotide (30 bases) was hybridized with the ssDNA template by annealing at 90 °C for five minutes in an annealing buffer. Unhybridized oligonucleotides were removed by centrifugation, and the hybridized DNA was solved in TE buffer. The solution was resuspended in a 0.5% formaldehyde solution and incubated with equivalent streptavidin-coated colloidal Au particles (5 nm diameter, Amersham) for five hours at room temperature. This resulted in the final concentrations of the DNA and the Au particles both being 10^{-9} M. The DNA-Au complexes were deposited on a Mg^{2+} coated mica substrate by placing 10 μl (one drop) of the DNA-Au solution on the substrate for five minutes. The solution was removed by blowing, and the samples were then observed by tapping-mode AFM (Seiko Instruments Inc.) in air.

A-3 Results and discussion

In aqueous solution, the nucleic acid bases make pairs in the same strand of the ssDNA molecule. That causes the higher ordered structure of ssDNA as shown in Fig. A-2(a). Formaldehyde in the solution, which prevents self hybridization, is essential for reduction of the secondary structure of ssDNA molecules (Fig. A-2(b)). Fig. A-3 shows AFM images indicating the effects of formaldehyde on the higher order structure of ssDNA. In Fig. A-3(a), the ssDNA deposited from the solution without formaldehyde gives the protrusion of 15 nm, which is much larger than the height of ssDNA (about 0.5 nm). In contrast, as shown in Fig. A-3(b), the formaldehyde in the ssDNA solution changes the protrusion of ssDNA to 0.5 nm, which is consistent with the height data of ssDNA previously reported by Thundat et al [6]. This suggests that formaldehyde is indispensable to AFM observation of the DNA based nano-structure using ssDNA.

An AFM image of a DNA-Au complex is shown in Fig. A-4(a). An Au particle is combined with the circular ssDNA as intended. When biotinylated oligonucleotide was not hybridized with a ssDNA template, AFM observation revealed that no DNA-Au complexes were present. This indicates that an Au particle can be combined with a ssDNA template molecule only when biotinylated oligonucleotides are present, as expected from Fig. A-1. The length of the ssDNA template in Fig. A-4(a) is about 600 nm, which is much shorter than the expected length of 7.2 kb ssDNA but consistent with other reports [6]. This suggests that the secondary structure of the ssDNA is not perfectly eliminated by a 0.5% formaldehyde solution.

Table 1
Yield of DNA-Au complex in the samples incubated with and without the probe DNA. *Au0*, *Au1* and *Au2* mean the ssDNA combined with no particle, one particle and more than two particles, respectively. Others means the complex including unidentified particles which are larger than 7 nm. The total sampling numbers are 46 and 93 for *With probe ssDNA* and *Without probe ssDNA*, respectively.

	Au0	Au1	Au2	Others
With probe ssDNA	67%	15%	4%	14%
Without probe ssDNA	90%	5%	1%	4%

The measured height of the Au particle is 4.6 nm, which is fairly close to the size of the Au particles used.

The conjugation of Au particle with ssDNA shows the variations. Figure A-5 shows an AFM image of ssDNA mixed with Au particles. The ssDNA observed can be classified into: (a) one Au particle combined with a ssDNA; (b) no Au particle combined with a ssDNA; (c) more than two Au particles combined with a ssDNA. This indicates the hybridization does not accrue completely. We examined the yield of DNA-Au complexes classified by the number of the combined particles whose size are ranged from 3 to 7 nm height. This size range is set to 99.99 % distribution of the colloidal Au particles. Furthermore, the yield was compared between the sample incubated with and without the probe ssDNA. In Table 1, *Au0*, *Au1* and *Au2* mean the ssDNA combined with no particle, one particle and more than two particles, respectively. *Others* means the complex including unidentified particles, which are larger than 7 nm height. With the probe ssDNA, the template ssDNAs combined with one particle (*Au1*) were generated at a rate of 15 %. The remainders can be classified *Au0* (67 %), *Au2* (4 %) and *Others* (14 %). On the other hand, without the probe ssDNA, *Au1* were counted at a rate of 5 % in the analysis of sectional profiles.

However, it was found that this yield appears due to the secondary structure because the feature in images is quite different from the Au particles. Accordingly, the Au particle can be combined with the ssDNA template molecule only under the existence of the probe ssDNA, as expected from Fig. A-1. This result derives the intrinsic reaction probability for the DNA-Au complex by the biotin-streptavidin reaction is about 10 % in this experiment.

A-4 Conclusion

The Au-DNA conjugation was controlled by Watson-Crick base pairing interaction and biotin-streptavidin interaction. The one-to-one binding of Au nano-particles to ssDNA molecules was confirmed by AFM. The yield of the one-to-one binding was about 10 %. This value is small to arrange several particles. These results, however, indicate that this method is useful for the controlled arrangement of Au nano-particles on a ssDNA template. Further improvements are required in reducing the secondary structure and fixing the ssDNA on a substrate. This approach, however, would provide a new strategy for the fabrication of DNA-based nano-structures suitable for a wide range of applications.

A-5 References

[1] E. Braun, Y. Eichen, U. Sivan, G. Ben-Yoseph: Nature **391** (1998) 775

[2] C.A. Mirkin, R.L. Letsinger, R.C. Mucic, J.J. Storhoff: Nature **382** (1996) 607

[3] A.P Alivisatos, K.P Johnsson, X. Peng, T.E. Wilson, C.J. Loweth, M.P. Bruchez Jr., P.G. Schultz: Nature **382** (1996) 609

[4] W.-L. Shaiu, J. Vesenka, D. Jondle, E. Henderson, D.D. Larson: J. Vac. Sci. Technol. A**11** (1993) 820

[5] J.E. Coury, L. McFail-Isom, S. Presnell, L.D. Williams, L.A. Bottomley: J. Vac. Sci. Technol. A**13** (1995) 1746

[6] T. Thundat, D.P. Allison, R.J. Warmack: J. Vac. Sci. Technol. A**11** (1993) 824

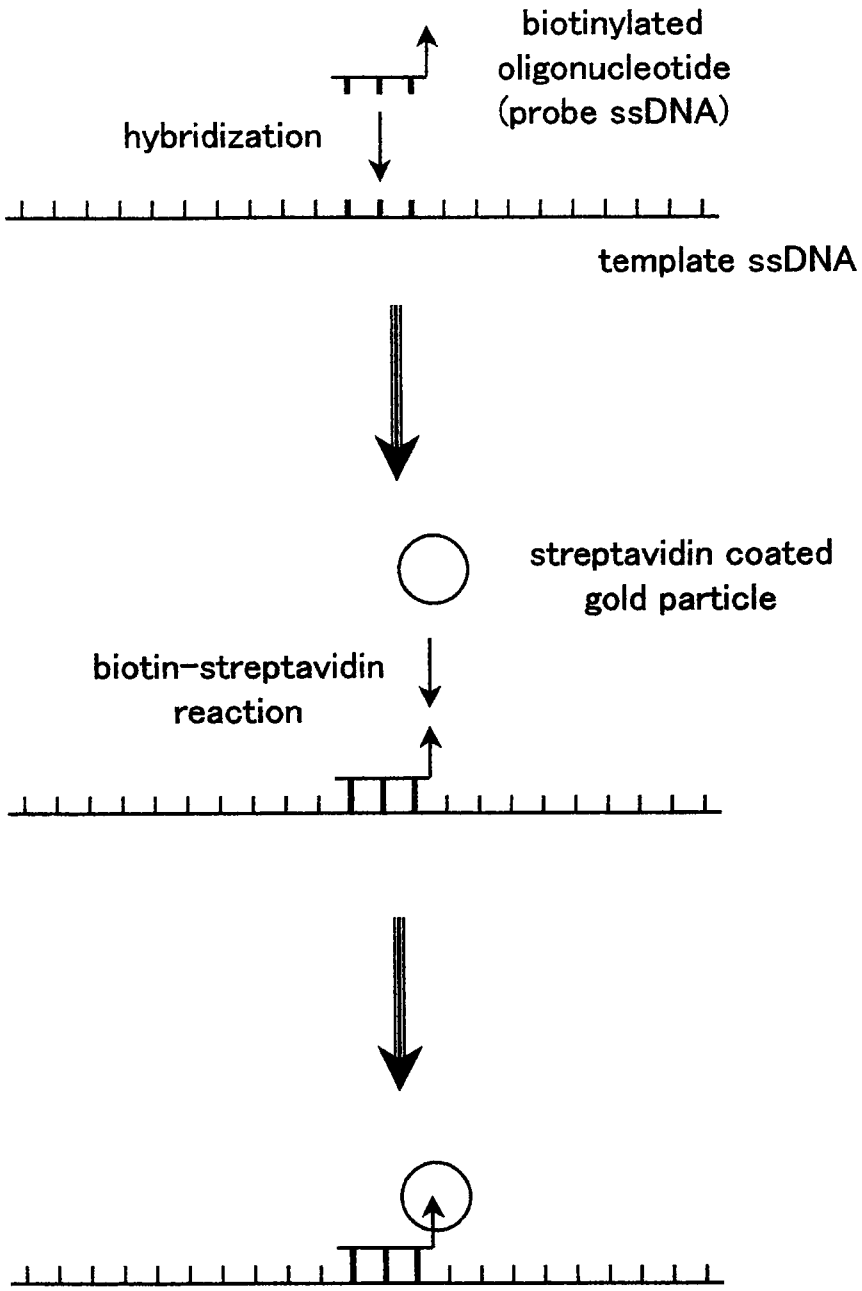

Fig. A-1
Strategy for the controlled addition of an Au particle to a template single-stranded DNA (ssDNA) molecule. A biotinylated oligonucleotide (probe DNA) is hybridized with the template ssDNA molecule. A streptavidin coated Au particle (5 nm diameter) is bonded to the probe ssDNA by a biotin-streptavidin reaction.

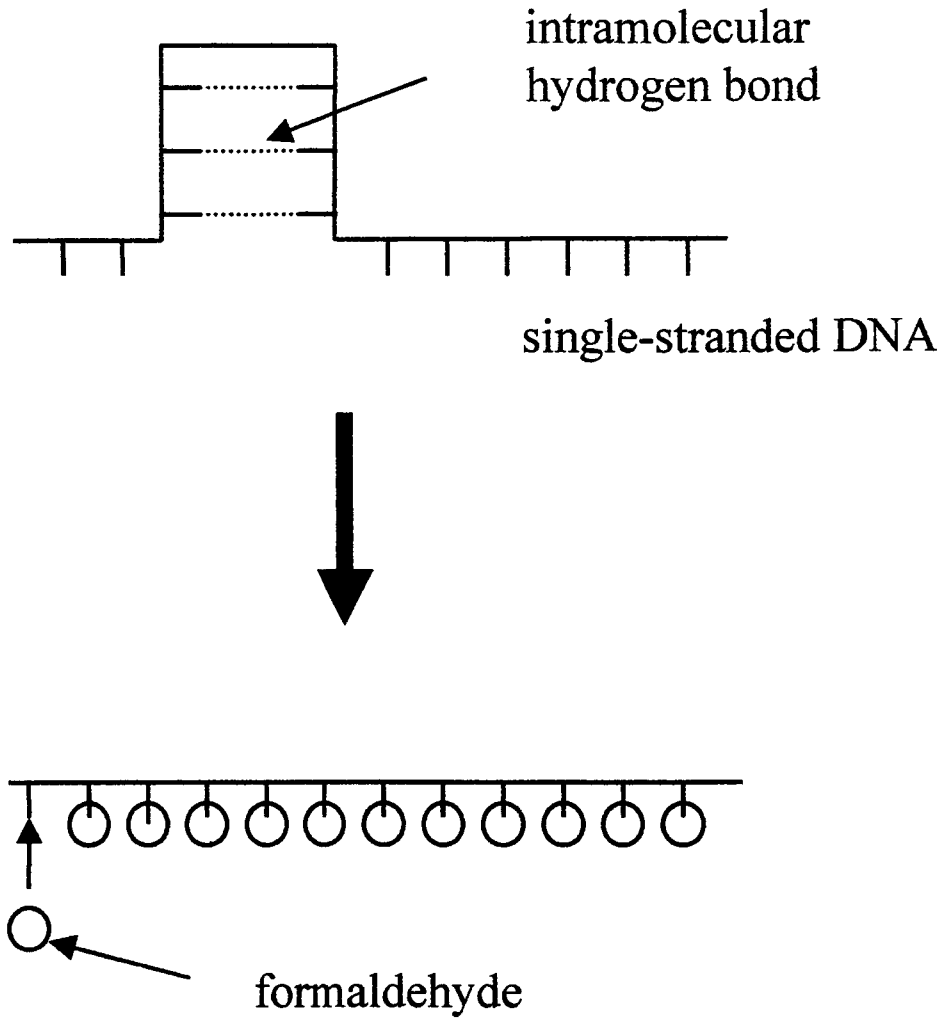

Fig. A-2
Schematic illustration of the effect of formaldehyde.

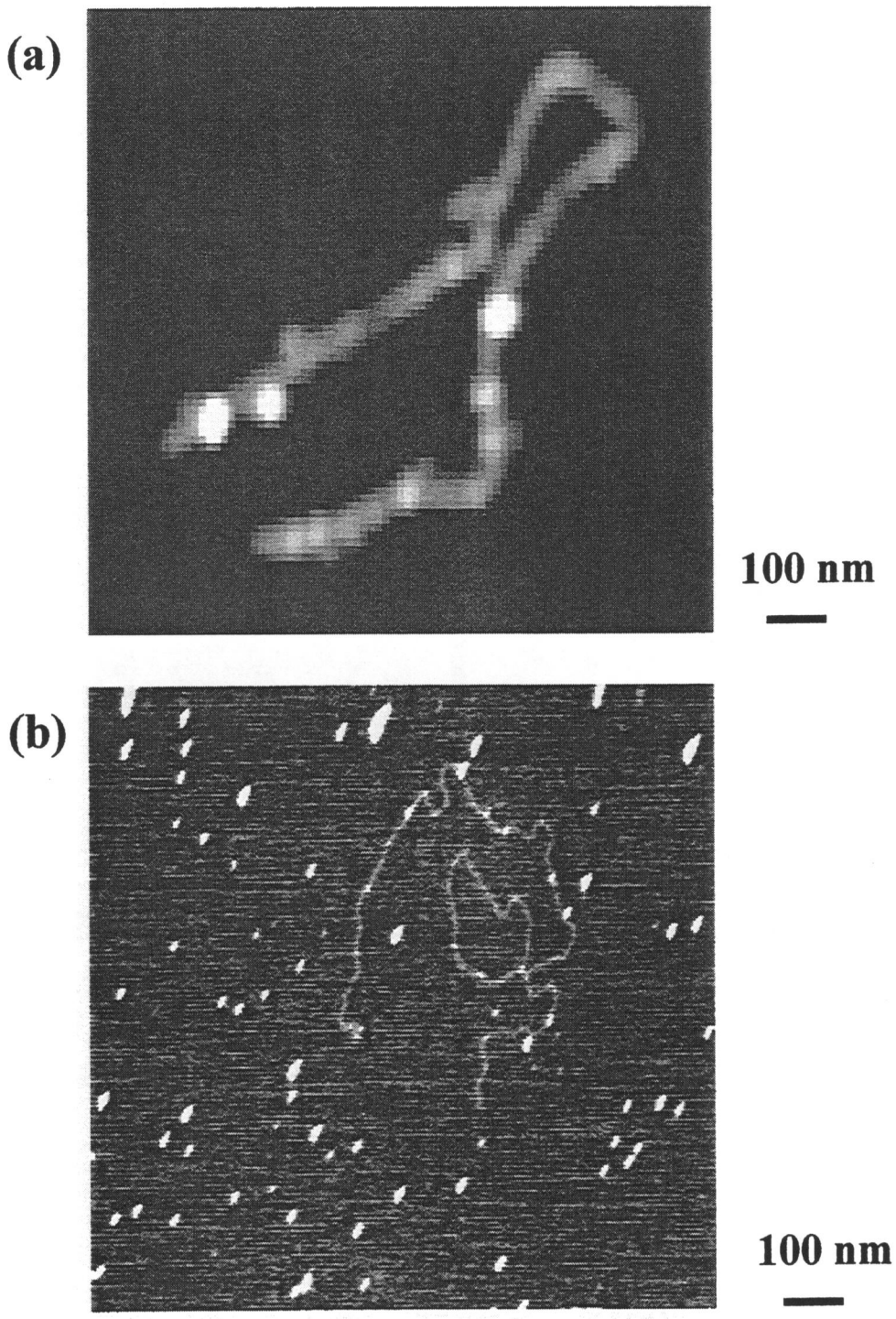

Fig. A-3
(a) AFM image of a single-stranded DNA (ssDNA) molecule deposited from aqueous solution. The height of the single-stranded DNA is 15 nm. (b) AFM image of ssDNA deposited from 0.5 % formaldehyde aqueous solution. The height of ssDNA molecule is 0.5 nm.

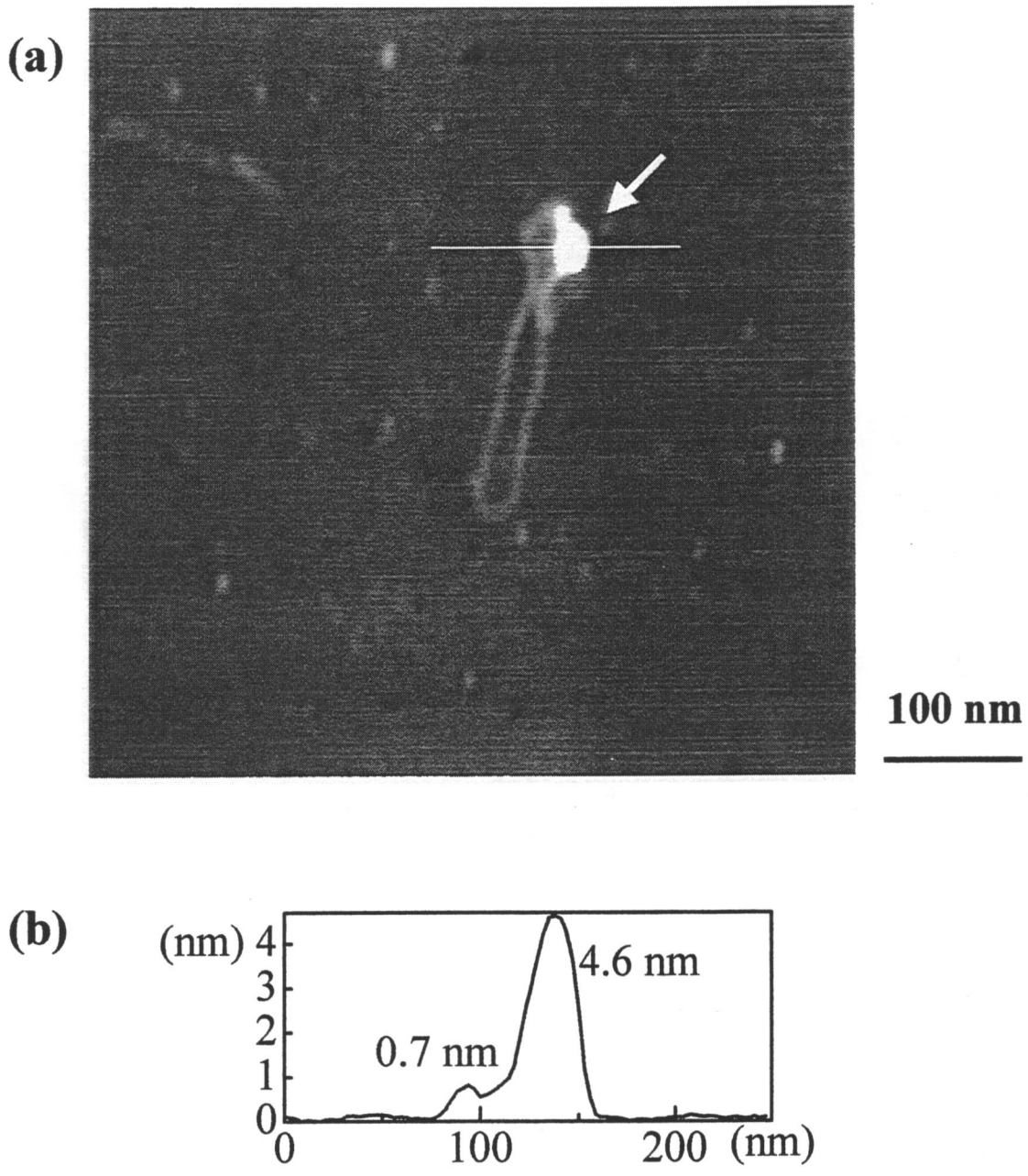

Fig. A-4
(a) AFM image of an Au-DNA conjugation. The Au particle is marked with arrow. (b) The sectional profile across the Au particle at the line indicated in (a). The height of the single-stranded template DNA and the Au particle are 0.7 nm and 4.6 nm, respectively.

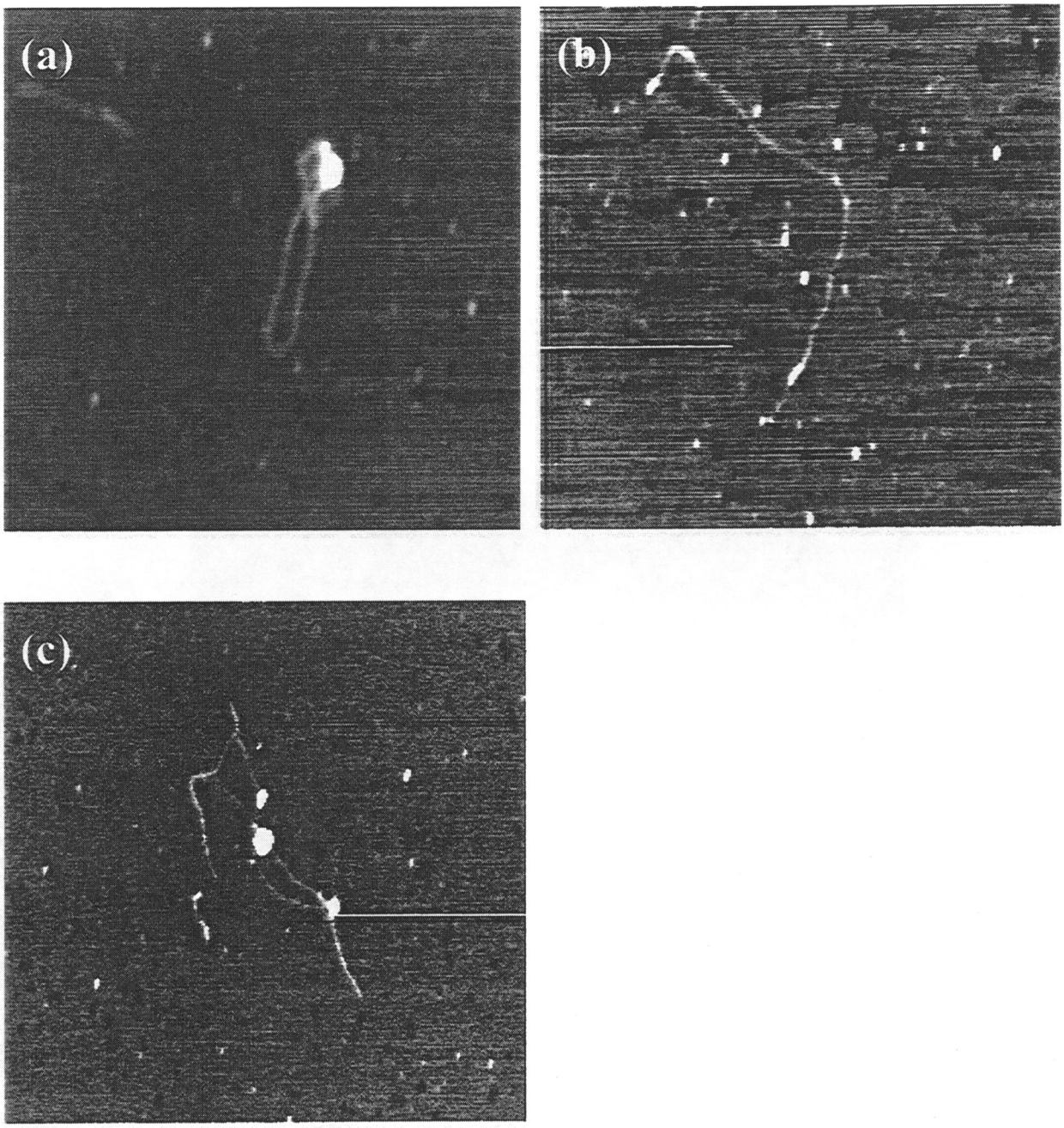

Fig. A-5
AFM images of products. A template DNA is combined with (a) a Au particle, (b) no Au particle and (c) more than two Au particles.

List of Publications

1. "Adsorption structure of copper-phthalocyanine molecules on Si(100) 2x1 surface by scanning tunneling microscopy."
Y. Maeda, T. Matsumoto, M. Kasaya, T. Kawai
Japanese Journal of Applied Physics **35** (1996) L405.

2. "Photoexcited carrier effect on imaging of organic molecules on Si(100) 2x1 surface."
Y. Maeda, T. Matsumoto, T. Kawai
Material Research Society Symposium Proceedings, Boston U.S.A Dec. 2-6 (1996).

3. "Photoexcited carrier effect on scanning tunneling microscopy of Zinc-phthalocyanine and coronene molecules on Si(100) 2x1 surface."
Y. Maeda, T. Matsumoto, T. Kawai
Surface Science Letters **384** (1998) L896.

4. "Observation of single- and double-stranded DNA using non-contact atomic force microscopy."
Y. Maeda, T. Matsumoto, T, Kawai
Applied Surface Science **140** (1999) 400.

5. "Frequency-modulation SFM imaging of DNA molecules in UHV conditions."
Y. Maeda, T. Matsumoto, T. Kawai
Surface and Interface Analysis **27** (1999) 450.

6. "Controlled conjugation of nanoparticles with single-stranded DNA."
Y. Maeda, T. Nakamura, K. Uchimura, T. Matsumoto, T. Kawai
Journal of Vacuum Science and Technology **B17** (1999) 494.

7. "Atomic force microscope observation of plasmid deoxyribose nucleic acid with restriction enzyme."
T. Nakamura, Y. Maeda, T. Oka, H. Tabata, M. Futai, T. Kawai
Journal of Vacuum and Technology **B17** (1999) 288.

8. "High-resolution imaging of DNA under ultrahigh vacuum conditions by non-contact atomic force microscopy."
T. Matsumoto, Y. Maeda, T. Kawai
Journal of Vacuum Science and Technology **B17** (1999) 1941.

9. "Imaging of the DNA double helix structure by noncontact atomic force microscopy."
Y. Maeda, T. Matsumoto, H. Tanaka, T. Kawai
Japanese Journal of Applied Physics Express Letter **38** (1999) L1211.

10. "Electrostatic force at mica surfaces probed by frequency-shift spectroscopy."
Y. Naitoh, Y. Maeda, T. Matsumoto, T. Kawai
Surface Science Letters in press

11.「走査プローブ顕微鏡によるDNA分子の観察」
前田泰、川合知二
エレクトロニクス・コミュニケーション(Electronics Communications)誌、15号、
p19-23 (2000)

Acknowledgement

I am greatly indebted to Professor T. Kawai of ISIR-Sanken, Osaka University for his encouragement and continuing guidance throughout the course of this investigation.

I am grateful to Assistant Professor T. Matsumoto for his valuable discussions and helpful suggestions during this study.

It is a great pleasure for me to have two supervisors for this thesis, Professor T. Kasai of Department of Chemistry, Osaka University and Professor H. Watarai of Department of Chemistry, Osaka University.

I would like to thank Assistant Professor H. Tabata and Dr. H. Tanaka for their helpful discussions and advice on the fabrication of DNA based nano-structure and the imaging mechanism of SPM.

I wish to thank Mr. Y. Naitoh and Mr. S. Okochi for their support and helpful discussion on NC-AFM observation.

I wish to thank students belonging to the laboratory under the direction of Professor T. Kawai of ISIR-Sanken, Osaka University.

Finally, I express my special thanks to my family for their heartiest supports.